

# **Nanomechanics of Soft and Living Matters**

**Sujal Kataria**

*A dissertation submitted for the partial fulfilment of BS-MS dual degree in  
Science*



**Department of Physics,  
Indian Institute of Science Education and Research, Pune**

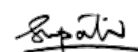


## Certificate of Examination

This is to certify that the dissertation titled **Nanomechanics of soft and live matters** submitted for the partial fulfillment of BS- MS Dual Degree programme of the Indian Institute of Science Education and Research, Pune represents study/work carried out by **Sujal Kataria** (Reg. No. 20191023), under the supervision of “Prof. Shivprasad Patil, Professor, Department of Physics”.



Sujal Kataria  
20191023

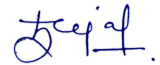


Prof. Shivprasad Patil  
(Supervisor)



## **Declaration**

I hereby declare that the matter embodied in the report entitled “Nanomechanics of soft and live matters” are the results of the work carried out by me at the Department of Physics, Indian Institute of Science Education and Research (IISER) Pune, under the supervision of Prof. Shivprasad Patil, and the same has not been submitted elsewhere for any other degree. Wherever others contribute, every effort is made to indicate this clearly, with due reference to the literature and acknowledgement of collaborative research and discussions.



Sujal Kataria

20191023

In my capacity as the supervisor of the candidates project work, I certify that the above statements by the candidate are true to the best of my knowledge.

Prof. Shivprasad Patil  
(Supervisor)



## Acknowledgements

This thesis is dedicated to my parents, whose unwavering love and support have been the foundation of my journey.

I extend my heartfelt gratitude to my supervisor, Prof. Shivaprasad Patil, for his invaluable guidance and encouragement throughout this research endeavour. Under his mentorship, I cultivated a curious and problem-solving mindset, which has been instrumental in shaping my academic pursuits. Prof. Shiva's chill attitude and willingness to give us full freedom to work created a creative environment. His thoughtful gestures, such as inviting us to parties and festivals at his home and cooking dishes for us, made us feel like cherished members of his extended family. Moreover, his unwavering availability to assist has been truly remarkable and deeply respected.

I am also grateful to Dr. Nagraj for his insightful discussions and constructive feedback, which greatly enriched my understanding of the subject. Special thanks to Dr. Vijayakumar Chikkadi for sharing his valuable time as expert for my thesis.

I deeply appreciate my senior lab members, Dr. Shatruhan and Dr. Surya, for their constant guidance and availability whenever I encountered obstacles. Their mentorship has been invaluable in navigating the challenges during the thesis.

To Lokendra, Vidushi, Manish, Pratishruti, Hrishikesh, and all my friends who have supported me throughout my college journey, I am immensely grateful for your unwavering friendship and encouragement.

I extend my gratitude to my current lab mates, including Shrikrishna, Hrishikesh, Vishal, Swarnaow, and Vedant, whose camaraderie has made my lab enjoyable and productive.

I would also like to acknowledge the support of my school friends, especially Mahak, for their enduring friendship and support over the years.

A heartfelt thank you to my collaborators, Surya bhaiya from NCCS, Debasmita, and Virendra sir, for their assistance whenever I reached out for help.

Special thanks to Vidushi and Lokendra for their unwavering support and guidance, which helped me navigate the highs and lows of college life with resilience.

Lastly, I am profoundly grateful to my papa, mamma, maa, baba and jiya for their boundless love, care, and unwavering support throughout my academic journey. Their encouragement has been my source of strength and motivation.

# CONTENTS

<b>1</b>	<b>Atomic Force Spectroscopy (AFM)</b>	<b>14</b>
1.1	Introduction of AFM . . . . .	14
1.2	Modes of AFM . . . . .	16
1.3	Experiments with AFM . . . . .	17
1.4	AFM for this thesis . . . . .	18
1.5	Other Techniques . . . . .	20
1.5.1	Magnetic Tweezers . . . . .	20
1.5.2	Optical Tweezers . . . . .	21
1.5.3	Advantages of Atomic Force Microscopy (AFM) . . . . .	21
1.6	Plan of thesis . . . . .	22
1.7	Abstarct . . . . .	23
<b>2</b>	<b>Molecular interaction of SARS-CoV-2 mutants binding to the human ACE2 receptor using AFM</b>	<b>25</b>
2.1	Introduction . . . . .	25
2.2	Methods . . . . .	29
2.2.1	Gold coating of glass coverslips . . . . .	29
2.2.2	Preparation of ACE2-coated gold surfaces . . . . .	30
2.2.3	Functionalization of AFM tips . . . . .	30
2.2.4	FD-based AFM on model surfaces . . . . .	33
2.3	Results and Discussion . . . . .	33
2.4	Future Plans . . . . .	37
<b>3</b>	<b>Measuring Viscoelastic properties of L-cells lacking clathrin light chains.</b>	<b>39</b>
3.1	Introduction . . . . .	39
3.2	Methods and Materials . . . . .	44
3.2.1	Bead attachment . . . . .	44
3.2.2	Nanoindentation experiments . . . . .	45
3.2.3	Data Analysis . . . . .	46
3.2.4	Sourcing of L cells . . . . .	46



3.3	Results and Discussion . . . . .	46
<b>4</b>	<b>Quantitative evaluation of collagen organisation and its regulation by mouse fibroblasts in 3D hydrogels using AFM</b>	<b>48</b>
4.1	Introduction . . . . .	48
4.2	Methods . . . . .	51
4.2.1	Sourcing of Cells, Phenotype and Gel . . . . .	51
4.2.2	AFM Investigation of Collagen Gel . . . . .	51
4.2.3	AFM Investigation of MEFs Cells . . . . .	51
4.2.4	Analysis of Elasticity Data . . . . .	51
4.3	Results and Discussion . . . . .	51
<b>5</b>	<b>Conclusion</b>	<b>57</b>

## LIST OF FIGURES

1.1	Figure showing deflection detection schematic of an commercial AFM, A laser beam reflects from the back of the cantilever and collected at the position-sensitive photo-detector, Figure Credits: Dr. Shatruhan. . . . .	14
1.2	Figure showing, Laser-alignment in optical beam deflection detection. A laser beam fall on the back of the cantilever through a prism and adjusted by mirror to fallo on photo detector, Figure Credits: Dr Shatruhan . . . . .	15
1.3	A Force-Displacement (FD) curve, The red color is approach and the dark red curve is retract. This particular curve corresponds to experiment with Omicron protein on cantilever and Receptor protein on coverslip and we can clearly see the deflection in retract curve which is due to protein-protein interaction. . . .	19
2.1	(a) The schematic of a SARS-CoV-2 virus depicts the expression of the spike glycoprotein (S) on its surface. This spike protein is crucial in facilitating the virus's binding to host cells. (b) Structural studies have revealed a complex interaction between the receptor-binding domain (RBD), a subunit of the spike glycoprotein, and the Angiotensin-Converting Enzyme 2 (ACE2) receptor. This interaction is fundamental for the virus to enter host cells and initiate infection. (c) A schematic representation illustrates the use of atomic force microscopy (AFM) to probe the binding of SARS-CoV-2 to its target molecules. In this method, interactions between the virus and its receptor are monitored by AFM on model surfaces. The ACE2 receptor is immobilized on a surface, while the S1 subunit of the mutants is attached to the AFM tip. Source: [34]. . . .	26
2.2	(A) A schematic representation of the SARS-CoV-2 spike protein highlights its various domains, each depicted in distinct colors. These domains play crucial roles in the protein's structure and function. (B) The cryo structure of the SARS-CoV-2 spike protein illustrates two conformational states: the closed state (left) and the open state (right) of the S glycoprotein. These states represent different configurations of the spike protein, which are essential for its interactions with host cell receptors and the fusion process during viral entry. Figure Source: [31]. . . . .	27

2.3	Figure(a) showing FD curve on gold surface with no interaction with ACE-2 (non adhesive contact) and Figure (b) showing FD curve showing deflection due to rupture of S1 and ACE-2 on surface with green curve is WLC fitting. . .	28
2.4	Functionalization steps to attach Linker molecule SPDP-(dPEG)36-NHS ester on Gold surface common for coverslip and cantilever . . . . .	31
2.5	Functionalization steps to attach protein after Linker molecule is attached on Gold surface common for coverslip and cantilever . . . . .	32
2.6	Figure showing AFM topography image of an ACE2 coated surface after scanning a 1 $\mu\text{m}$ x 1 $\mu\text{m}$ area at high forces (around 18 nN) and 5 $\mu\text{m}$ x 5 $\mu\text{m}$ imaged at very low force. We can clearly see a blacked out spot which confirms the attachment of Linker on the gold surface . . . . .	33
2.7	Histogram of rupture length for the S1-subunit and ACE2 interaction (N = 64 data points). Multippeak Gaussian fit reveals a maximum of the rupture force at 28 +- 9 nm for the S1-ACE2 interaction . . . . .	34
2.8	Figure showing the histograms of rupture forces for the 6 different set of loading rates and a gaussian is fitted of Wuhan variant. The maximum of the fit is used fit the straight line in the loading rate vs rupture force plots to get its intercept and slope to find the $x_u$ and $k_{off}$ respectively. . . . .	36
2.9	Figure showing the loading rate vs rupture force distribution for the Wuhan variant and the black dots are the maximum from the histograms plotted above and the grey dots are from the WLC fit from the FD curves taken at different retract speeds. The intercept and slope is extracted from the straight line which will be used to find the $x_u$ and $k_{off}$ of the interaction. . . . .	36
2.10	Figure showing the histograms of rupture forces for the 6 different set of loading rates and a gaussian is fitted of Omicron variant. The maximum of the fit is used fit the straight line in the loading rate vs rupture force plots to get its intercept and slope to find the $x_u$ and $k_{off}$ respectively. . . . .	37
2.11	Figure showing the loading rate vs rupture force distribution for Omicron variant and the black dots are the maximum from the histograms plotted above and the grey dots are from the WLC fit from the FD curves taken at different retract speeds. The intercept and slope is extracted from the straight line which will be used to find the $x_u$ and $k_{off}$ of the interaction. . . . .	37
3.1	Clathrin light chain a and b knockout was made in L cells with the help of CRISPR/ Cas9. Here, green is phalloidin, which stains F actin. Actin patches are more prominent in clathrin light chain a and ab double knockouts than in the wild type. Image Credit: Surya Bansi, Dr Deepa's Lab, NCCS . . . . .	41

3.2	Figure showing a plot of Tip position vs Deflection) with a Approach (Light Red) and Retract (Dark Red) curve on cell with the green curve is Hertz Fit. The hysteresis between approach and retract part is used to calculate the viscoelastic Parameters. . . . .	43
3.3	Fig. shows The tip, with a bead glued on it, interacts with the sample, and the interaction forces cause the microcantilever to deflect (bend) and the deflection on cantilever is read by the photodetector Source: [28]. . . . .	44
3.4	Fig. shows stepwise protocol to attach bead on cantilever as explain above. Source: [28]. . . . .	45
3.5	Figure showing Box plot of Young's Modulus comparison of WT, Clta, Cltb and Cltab . . . . .	47
3.6	Figure (A) showing box plot of E0 values of L cells and corresponding clathrin light chain knockout phenotypes and Figure (B) showing box plot of alpha values of L cells and corresponding clathrin light chain knockout phenotypes. . . . .	47
4.1	3D Collagen hydrogel – Reflectance Imaging, Difference in branch number with changing the concentration of collagen. Figure Credits: Debasmita Mazumdar from Dr Nagraj Lab . . . . .	50
4.2	Figure showing a plot of Tip position vs Deflection with a Approach (Light Red) and Retract (Dark Red) curve on single cell. . . . .	52
4.3	Figure shows two plots left is the comparison of stiffness of WT MEFs with 3 different concentrations of Lat A along with there reflectant images on top of the plots similarly on right is the comparison of stiffness of Cav Null MEFs with 3 different concentrations of Lat A along with there reflectant images on top of the plots. Image Credits: Debasmita Mazumdar from Dr Nagraj Lab . . . . .	53
4.4	Figure stiffness change on adding Rock Inhibitor of two different concentration. . . . .	53
4.5	Figure shows two plots. The left plot shows the stiffness difference even when cells are round that is when the coverslip is coated with poly l lysine. The right plot shows plot that confirms at the 0.25uM Lat A the stiffness of both are same. This information will be used in further analysis. . . . .	54
4.6	Figure shows that for WT MEFs at the higher concentration, both the branch number and junctions were lower compared to the lower concentration on the other hand embedding Cav-1 Nulls did not show any significant difference in branch number or junctions across the two collagen concentrations. Figure Credits: Debasmita Mazumdar from Dr Nagraj Lab . . . . .	55

4.7 Figure shows that for WT MEFs and Cav-1 Nulls both treated with Lat A did not show any significant difference in branch number or junctions across the two collagen concentrations and is comparable as there was no cell embedded inside the gel. Figure Credits: Debasmita Mazumdar from Dr Nagraj Lab . . . 56

## Chapter 1

### ATOMIC FORCE SPECTROSCOPY (AFM)

#### 1.1 INTRODUCTION OF AFM

Atomic Force Microscope (AFM) is a member of the scanning probe microscope (SPM) family. It was invented by Gerd Binnig, Calvin Quate, and Christoph Gerber in 1986 [3]. Their motivation for this invention was to do morphology studies of poorly conducting surfaces which cannot be done by Scanning Tunneling Microscope (STM) [4]. In AFM, a cantilever-tip assembly is used as a force sensor where the tip interacts with the sample, causing the bending of the cantilever. The bending of the cantilever can be measured using different detection schemes such as:

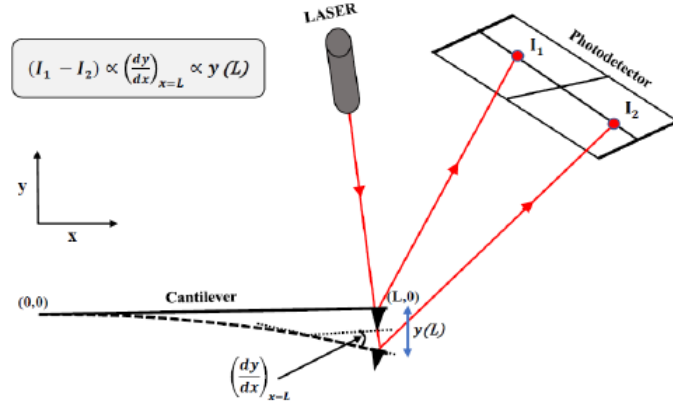


Figure 1.1: Figure showing deflection detection schematic of an commercial AFM, A laser beam reflects from the back of the cantilever and collected at the position-sensitive photodetector, Figure Credits: Dr. Shatruhan.

#### 1. Optical Beam Deflection:

This is the most common method, utilizing a focused laser beam reflected off the back of the cantilever. As the beam bends due to interaction forces, the reflected beam position changes, detected by a position-sensitive photodetector (PSD) see figure 1.1. The deflection of the re-

flected beam is proportional to the bending of the cantilever, allowing for the calculation of the applied force.

## 2. Capacitive Detection:

This technique utilizes changes in capacitance between the cantilever and a fixed electrode placed nearby. As the cantilever bends, the distance between them changes, altering the capacitance. This change in capacitance can be converted to voltage changes, which are then correlated with the bending and applied force.

## 3. Interferometry:

This technique utilizes the interference phenomenon between light beams to measure the bending of the cantilever with high sensitivity. By splitting a laser beam and directing one part onto the cantilever and the other onto a reference surface, the relative phase shift between the beams due to bending can be measured.

The detection system that our AFM is based on is Optical Beam Deflection.

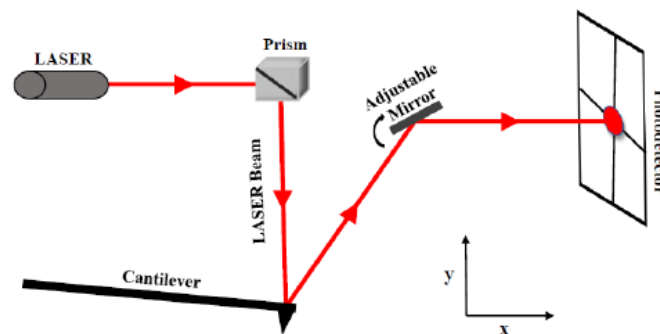


Figure 1.2: Figure showing, Laser-alignment in optical beam deflection detection. A laser beam fall on the back of the cantilever through a prism and adjusted by mirror to fallo on photo detector, Figure Credits: Dr Shatruhan

For small bending, force between the tip and sample can be estimated using Hook's law:

The equation represents the relationship between force ( $F$ ), the force constant of the cantilever beam ( $k$ ), and bending ( $y$ ), and it is given by:

$$F = k \cdot y \quad (1.1)$$

AFM is capable of measuring forces of the order of 10-1000s of piconewtons (pN). The capability of measuring such low to 1000s of pN force makes AFM a versatile tool and it has

been widely used to get surface morphology with atomic/molecular resolution, to quantify the Inter-Molecular forces between the tip and substrate, to measure forces in the biomolecules, Single Cellular Mechanics and Single Protein-Protein Interactions.

Further discussion will be mainly focused on the application of the AFM in Single Cellular Mechanics and Protein-Protein Interactions.

## **1. Cellular Mechanics:**

AFM allows precise measurement of mechanical properties at the single-cell level, offering insights into cell adhesion, stiffness, and viscoelasticity. By probing on the cell membrane, We can get the approach and retract curves (called nano-indentation) further analysing them can provide valuable data on cellular response for the understanding of cell biomechanics.

## **2. Protein-Protein Interactions:**

AFM also serves as a powerful tool for investigating protein-protein interactions. By functionalizing the AFM tip with specific ligands/linkers, we can selectively probe the binding forces between biomolecules immobilized on the substrate surface (coverslips). This enables the quantification of binding affinities, thermodynamics and kinetics of the interactions.

## **1.2 MODES OF AFM**

To perform experiments AFM can be operated in two modes: Static Mode and Dynamic Mode.

### **1. Static Mode (Contact Mode):**

In this mode, the AFM tip remains in constant contact with the sample surface, exerting a constant force during scanning. Static mode is well-suited for high-resolution imaging of surface morphology with atomic or molecular resolution, providing detailed topographical information of cellular structures and protein assemblies. In Cellular Mechanics, Static Mode AFM facilitates the characterization of cell surface features, using nanoindentation in which the approach and retract curves on individual live cells is taken and analysed further to extract mechanical properties like elasticity. This involved maintaining a constant approach and retract speeds of  $2\mu\text{m/s}$  over an area of  $1 \times 1\mu\text{m}^2$  onto cells. Moreover, in studies of Protein-Protein Interactions, Static Mode AFM enables us to quantify inter-molecular forces and by analyzing the deflection of the cantilever as it interacts with the surface, We can deduce the magnitude and distribution of forces acting between proteins. This capability allows us for the precise measurement of, rupture forces, rupture lengths and etc.



## **2. Dynamic Mode (Tapping Mode):**

Dynamic mode involves oscillating AFM cantilever near its resonant frequency while scanning the sample surface. By monitoring the amplitude and phase shift of the oscillation, dynamic mode allows for sensitive detection of surface interactions and mechanical properties without causing damage to the sample. This is useful when we want to image with low forces and etc. I have used Static Mode AFM for the studies.

## **1.3 EXPERIMENTS WITH AFM**

Prior to acquiring data through Atomic Force Microscopy (AFM), We need to perform some of preliminary process that are:

### **1. Cantilever and Substrate Mounting:**

The selected cantilever, carefully chosen based on the intended experiment and desired measurements. With careful handling to avoid damaging to the delicate cantilever is safely secured onto the designated cantilever holder.

The sample referred to as the "substrate," such as cells or immobilized proteins is precisely positioned onto a coverslip within a designated coverslip holder.

### **2. Calibration:**

The AFM system is calibration before data acquisition. This step involves establishing a precise correlation between the measured signal from the detection system and the actual force exerted by the cantilever on the sample[17]. Following is the breakdown of the calibration process:

#### **2.1. Sensitivity Calibration:**

This process establishes the conversion factor between the voltage signal measured by the detection system (e.g., Optical Beam Deflection) and the actual force applied to the cantilever (usually in nanonewtons). This conversion factor is often determined by experimentally applying known voltage to the cantilever while monitoring the corresponding response.

#### **2.2. Stiffness of cantilever:**

The spring constant ( $k$ ) of an AFM cantilever is a crucial parameter that determines the relationship between the applied force and the resulting deflection of the cantilever. Spring constant is essential for reliable force measurements in Atomic Force Microscopy (AFM) experiments and required for further calculations.

The thermal noise method is used for calibrating the spring constant of AFM cantilevers.[18]

This method utilizes the inherent thermal fluctuations experienced by the cantilever due to the random movement of its atoms caused by thermal energy.

In non-contact mode, meaning the cantilever does not physically touch the sample surface, the position of the cantilever tip is continuously monitored by the detection system using Optical Beam Deflection. The thermal fluctuations cause the cantilever to undergo small, random movements, which are reflected in the recorded position data. The recorded position data is used to calculate the mean-squared amplitude ( $\langle x^2 \rangle$ ) of the thermal noise, which represents the average squared displacement of the cantilever tip from its equilibrium position.

According to the Equipartition theorem, the average thermal energy ( $k_B T$ ) of a system in thermal equilibrium is proportional to its absolute temperature (T) and the Boltzmann constant ( $k_B$ ). This thermal energy is balanced by the potential energy stored in the cantilever due to its bending caused by the thermal fluctuations.

By equating the average thermal energy to the potential energy stored in the cantilever, we can derive the following equation:

$$k = \frac{k_B T}{\langle x^2 \rangle} \quad (1.2)$$

This equation relates the spring constant (k) to the measured temperature (T) and the mean-squared amplitude ( $\langle x^2 \rangle$ ) of the thermal noise.

After the calibration procedures, We are set for data acquisition in AFM.

## **The data acquisition**

It is started by approaching the cantilever towards the substrate surface. As the cantilever tip approaches the surface, the system continuously monitors the cantilever deflection and the corresponding vertical displacement as the tip approaches, contacts, and retracts from the surface. This information is captured as a Force-Displacement (FD) curve see figure 1.3, The acquired FD curve serves as a source of information about the sample's properties. By analyzing specific features of the curve, we can extract various parameters like Adhesion forces, Surface stiffness, Viscoelasticity, Rupture forces and etc.

## **1.4 AFM FOR THIS THESIS**

The AFM has elements like detection system, cantilever and its holder, cantilever motion controller, feedback circuit, data acquisition display unit.

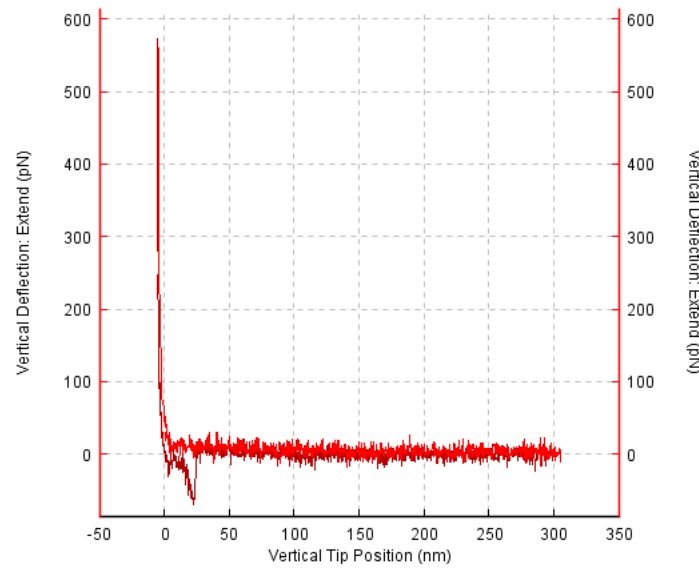


Figure 1.3: A Force-Displacement (FD) curve, The red color is approach and the dark red curve is retract. This particular curve corresponds to experiment with Omicron protein on cantilever and Receptor protein on coverslip and we can clearly see the deflection in retract curve which is due to protein-protein interaction.

### Detection system:

The AFM which is used utilizes a focused laser beam reflected off the back of the cantilever. As the cantilever interacts with the sample surface, its bending causes the reflected laser beam position to change, precisely measured by a position-sensitive photodetector. This deflection translates into the applied force and allows us for detailed analysis of sample and their properties.

### Cantilever Selection:

The projects involve three different sample types: Cells, Gels, and Single protein. Each sample presented specific modifications to the standard AFM cantilever:

**Cellular Experiments:** For these studies, the standard tipless cantilevers were modified by attaching small silica beads on their ends. This modification prevent excessive cellular damage as the contact area of the bead compared to a sharp tip significantly reduces the force applied to the cell surface, minimizing potential damage during measurements.

**Gel Experiments:** In contrast to cellular studies, larger beads were attached on cantilever for gel experiments. The rationale behind this modification is to prevent tip penetration into the Gels as the gels were very soft compared to cells.

**Protein-Protein Experiments:** For these experiments, the AFM cantilevers were used with the sharp tip. This is chosen for High resolution and sensitivity and Minimal steric hindrance,

The minimal size of the sharp tip minimizes steric hindrance, reducing the possibility of the tip interfering with the specific protein-protein interactions under investigation.

### **Motion control and Feedback circuit:**

Beyond the selection of AFM mode (that is static for our case) followed by cantilever selection and modification, several crucial parameters like the force to be applied(set-point), sampling rates, retract and approach speeds, ramp distances(z-lengths) were optimized for each experiment based on the specific sample type and the desired measurements. Some of them are briefly explained following:

**Approach/Retract Speeds:** The speed at which the AFM tip approaches and retracts from the sample surface significantly impacts the acquired data. For delicate samples like cells, slower approach speeds minimize the risk of damaging the cell during contact.

**Setpoint Force:** This parameter defines the constant force maintained between the cantilever and the sample surface during scanning in static mode AFM. Selecting an appropriate setpoint force is critical.

**Z-Length:** This parameter defines the total vertical range of movement for the AFM tip during scanning. An appropriate z-length ensures the tip properly scans the entire region of interest while avoiding unnecessary movement that could increase measurement time or introduce artifacts.

These specific values of all the parameters is mentioned in each chapter.

## **1.5 OTHER TECHNIQUES**

### **1.5.1 MAGNETIC TWEEZERS**

The first Magnetic Tweezers (MT) were assembled by Strick et al. in 1996. Magnetic Tweezers are capable to investigate the understanding of the elasticity of nucleic acids (DNA and RNA), [9] These vital biomolecules exhibit dynamic structures that change during their diverse functions. MT enables us to investigate these properties by applying controlled forces and observing the molecules' responses. Probing protein folding and unfolding, Studying the forces involved in protein conformational changes provides valuable insights into their functions and potential targets for drug development [11]. The working range on the force is 0.01 to 100 pN for MT but other single molecule force spectroscopic techniques do not allow measurements with such a low forces.

While magnetic tweezers (MT) offer a valuable tool for single-molecule force spectroscopy, they are not without limitations.

### 1.5.2 OPTICAL TWEEZERS

Optical tweezers (OT) was invented by the Arthur Ashkin and he received Nobel prize for this in 2018 [1]. Optical tweezers function on the principle of optically trapping micro-objects, a concept first demonstrated by Ashkin and his group in 1968. This technique has since become instrumental in studying single-molecule mechanics and biophysical phenomena at the nanoscale [6]. In an optical tweezers setup, a spherical bead is positioned at the focal point of a Gaussian laser beam, which is focused through a high numerical aperture lens. The bead, when situated precisely at the center of the beam, experiences optical forces along the direction of light propagation. These forces arise from the interaction between the incident laser light and the bead's surface, leading to a balanced trapping effect. Notably, due to the symmetric nature of refraction, the bead is also trapped in the direction normal to the light propagation.

OT is sensitive for the lower forces. Its force working range is 0.1 to 100 pN. This is a powerful technique to mimic the physiological forces which are actually of the order of few piconewtons. OT is vastly used to study the protein folding/unfolding thermodynamic and kinetic properties, it can also be used to study the mechanics of other biomolecules and micro-organisms. While optical tweezers (OT) offer a valuable tool for manipulating and studying microscopic particles, they possess certain limitations.

### 1.5.3 ADVANTAGES OF ATOMIC FORCE MICROSCOPY (AFM)

Advantages of Atomic Force Microscopy (AFM) over Magnetic Tweezers (MT) and Optical Tweezers (OT) for nanoindentation experiments and protein-protein interactions:

**Direct Force Measurement:** AFM offers the most direct measurement of the applied force on the sample during nanoindentation. MT and OT rely on the response of a tethered bead or trapped particle, introducing complexities in force calibration. AFM's direct contact approach provides a more accurate representation of the forces involved.

**High-Resolution Imaging:** AFM excels in providing high-resolution topographical information about the sample surface. This allows us to identify specific regions for nanoindentation and analyze post-experiment indentations.

**Versatility:** AFM can be used for nanoindentation experiments on a wide range of samples, including soft biological materials like cells and tissues.

**Force and Distance Control:** AFM provides precise control over both the applied force and the tip-to-sample distance during protein-protein interaction experiments. This allows for detailed analysis of the binding strength and unbinding dynamics at the molecular level. MT offers force control, but distance information is often inferred from bead movement, poten-

tially introducing less precise measurements. OT excels at distance control, but applying well-defined forces can be challenging.

**Sample Preparation:** Both MT and OT require careful sample preparation, but AFM offers greater flexibility in terms of sample types and surface modifications. MT is limited to samples that can be readily tethered with magnetic beads. OT can be limited by sample transparency and absorption characteristics.

In conclusion, AFM offers several key advantages over MT and OT for nanoindentation experiments and protein-protein interaction studies.

## **1.6 PLAN OF THESIS**

My thesis involves three projects each project written in form of a chapter and the last chapter is conclusion, in this chapter I have concluded the project on the preliminary analysis that has been done so far.

### **Chapter 2: Molecular Interaction of SARS-CoV-2 Mutants Binding to the Human ACE2 Receptor using AFM.**

This project is focused to study the interaction between the SARS-CoV-2 virus mutants (Wuhan and Omicron) and its cellular entry point, the human Angiotensin-Converting Enzyme 2 (ACE2) receptor. Utilizing AFM, the project aims to compare the binding strengths of the Wuhan strain and the highly transmissible Omicron variant of SARS-CoV-2 with the human ACE2 receptor. By analyzing the force-distance curves obtained through AFM measurements and fitting Bell-Evans model, the project aims to shed light on the specific molecular interactions that govern the binding between the viral spike protein and the ACE2 receptor.

### **Chapter 3: Viscoelastic measurements of L Cells and their Clathrin Light Chain Knock-out Variants using AFM Nanoindentation.**

This chapter explores the mechanical properties of L cells, specifically focusing on the role of clathrin light chain in cellular mechanics. Clathrin is a protein essential for the formation of clathrin-coated pits, crucial for various cellular processes like endocytosis. The project aims to quantify viscoelastic properties of L cells, using AFM-based nanoindentation, the project aims to quantify the viscoelastic properties of L cells. These properties can provide valuable insights into the overall mechanical behavior and functional state of the cells and phenotypes.

## **Chapter 4: Quantitative Evaluation of Collagen Organization and its Regulation by Mouse Fibroblasts in 3D Hydrogels using AFM.**

The final chapter of thesis investigates the role of mouse fibroblasts in regulating microenvironment inside three-dimensional (3D) collagen hydrogels. The project compares the organization and structure of collagen fibers within 3D hydrogels when embedded with wild-type mouse embryonic fibroblasts and caveolin-1 null mouse embryonic fibroblasts. Caveolin-1 is a protein involved in various cellular processes, and its absence can affect cell-matrix interactions. This information can provide valuable insights into the role of fibroblasts with and without caveolin in regulating the surrounding extracellular matrix.

Each chapter will delve deeper into the specific methodology, results, and discussion for each project, providing a comprehensive understanding of the research conducted.

### **1.7 ABSTARCT**

This section contain abstracts of projects done for completion of my MS thesis.

#### **Project 1: Molecular interaction of SARS-CoV-2 mutants binding to the human ACE2 receptor using AFM**

The main project of this thesis is dedicated to examining the intricate interaction dynamics of SARS-CoV-2 virus mutants, specifically the Wuhan strain and the highly transmissible Omicron variant, with their cellular entry point, the human Angiotensin-Converting Enzyme 2 (ACE2) receptor. Through the application of Atomic Force Microscopy (AFM), this study aims to meticulously compare the binding strengths of these variants with the ACE2 receptor, offering insights into their respective kinetic profiles. By analyzing force-distance curves obtained through AFM measurements and employing the Bell-Evans model, the project endeavors to unravel the specific molecular interactions playing the binding process between the viral spike protein and the ACE2 receptor. This comprehensive investigation not only deepens our understanding of viral-host interactions of mutants but also holds promise for informing the development of targeted vaccine strategies aimed at changed kinetic off rates of viral variants with small mutations. We have shown experimentally the decrease in kinetic off rate for omicron variant.

#### **Project 2: Viscoelastic measurements of L Cells and their Clathrin Light Chain Knockout Variants using AFM Nanoindentation**

The actin cytoskeleton plays an important role in various cellular and biological processes such as cell polarity, cell migration, and intracellular and extracellular trafficking, thereby main-

maintaining cell shape and structure of a cell. The role of actin in endocytosis is well established, particularly in the context of clathrin mediated endocytosis (CME). CME is the major endocytic pathway involved in the maintenance of mouse embryonic stem cell (mESC) pluripotency. The central component of CME is the clathrin triskelion, which is composed of three molecules of the clathrin heavy chain (CHC), each of which is associated with the smaller clathrin light chain (CLC). In mammals, there are two clathrin light chains, CLCa and CLCb whose individual physiological roles are poorly understood. CLCs have been shown to help recruit and organize actin to sites of endocytosis in differentiated cells, especially under conditions of high membrane tension. The organization of actin cytoskeleton is distinct in different cell type. Using the CRISPR-Cas9 genome editing system, we have generated CLC knock out L - cell lines. We show that in the absence of CLCa, CLCb or both the light chains shows reduction in viscoelasticity of cells.

### **Project 3: Quantitative evaluation of collagen organisation and its regulation by mouse fibroblasts in 3D hydrogels using AFM**

Cells surrounded by the extracellular matrix (ECM) can sense mechanical cues from their micro-environment that are converted to a biochemical signal and executed as a biological response such as alteration of protein expression (Intracellular) or remodelling of the extracellular matrix (Extracellular). 3D collagen hydrogels with changing collagen concentration and embedded wild-type mouse fibroblasts (WT MEFs) provide a controlled system to evaluate the cell-matrix interaction. A small change in collagen concentration affects collagen organization in 3D hydrogels and differentially affects collagen organization in gels embedded with cells. Caveolin-1 lined caveolae are plasma membrane-invaginated nano-domains that are mechanosensitive and play a vital role in cellular mechano-protection. Caveolin-1 deficient fibroblasts (Cav-1 Null MEFs) differentially remodel their immediate microenvironment compared to WT MEFs. The effect of the differential collagen organization by WT MEFs and Cav-1 Null MEFs in stiffness has been investigated by using AFM using soft cantilevers and large silicon bead glued on it, 3D hydrogels with variable collagen concentration at different time points has been studied.



## **Chapter 2**

# **MOLECULAR INTERACTION OF SARS-COV-2 MUTANTS BINDING TO THE HUMAN ACE2 RECEPTOR USING AFM**

### **2.1 INTRODUCTION**

A novel coronavirus (CoV) was identified as the cause of an outbreak of pneumonia in China in 2019, this was named Coronavirus Disease-19 (COVID-19). This Coronavirus, known as Severe Acute Respiratory Syndrome Coronavirus-2 (SARS-CoV-2), have similarities with SARS-CoV that caused pandemic in early 2000s. The COVID-19 outbreak has ended into a severe pandemic affecting not only the health of millions but a huge impact on global economics. The genome of SARS-CoV-2 is approximately 80 percent identical with the SARS-CoV [35].

The entry of coronavirus into host cells is facilitated by its transmembrane spike (S) glycoprotein, forming a homotrimeric on the viral surface [30]. Advances in structural biology have provided insights into the molecular architecture and dynamics of the SARS-CoV-2 S protein. Cryo-electron microscopy (cryo-EM) studies have elucidated the trimeric arrangement of S protein spikes protruding from the viral surface and imparting the characteristic "crown-like" appearance to coronaviruses (see figure 2.1) . High-resolution structural analyses have further delineated the conformational landscape of the S protein, revealing intricate details of receptor binding and membrane fusion.

The protruding spike (S) proteins are crucial for the virus's ability to infect host cells. The spike protein consists of three identical protein chains and is modified with sugar molecules. It is divided into two functionally distinct subunits.

The S1 subunit is responsible for recognizing and binding to specific receptors on the host cell's surface. It contains a N-Terminal Domain (NTD) that interacts with sugar receptors on the host cell for initial attachment and a Receptor-Binding Domain (RBD), It is the critical domain that directly binds to the host cell receptor. In the case of SARS-CoV-2, the RBD binds to the human ACE2 receptor. The RBD can exist in an "up" (open) conformation for receptor binding or in a "down" (closed) conformation (see figure 2.2).

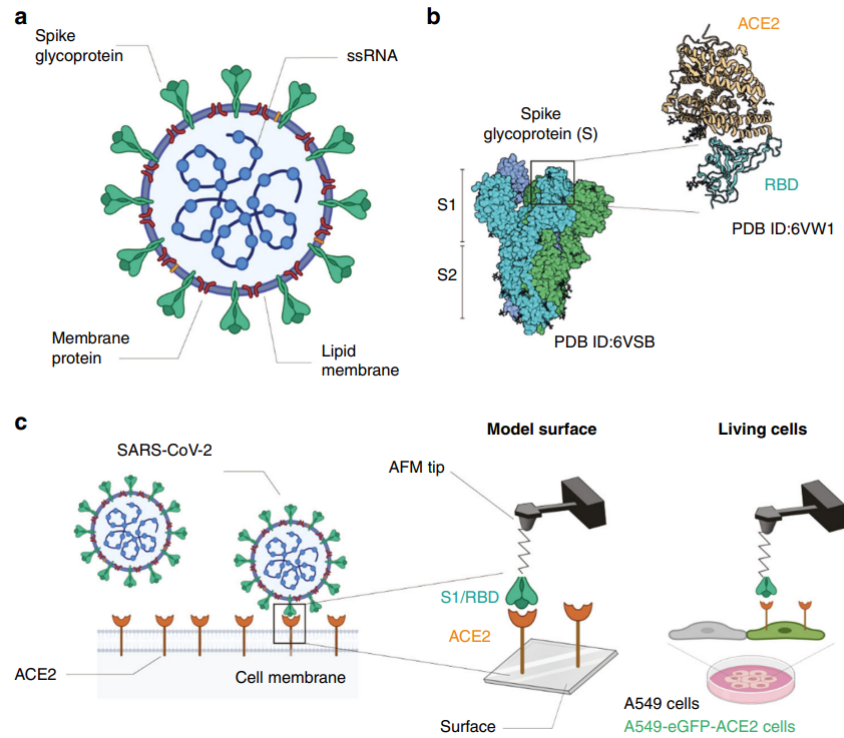


Figure 2.1: (a) The schematic of a SARS-CoV-2 virus depicts the expression of the spike glycoprotein (S) on its surface. This spike protein is crucial in facilitating the virus's binding to host cells. (b) Structural studies have revealed a complex interaction between the receptor-binding domain (RBD), a subunit of the spike glycoprotein, and the Angiotensin-Converting Enzyme 2 (ACE2) receptor. This interaction is fundamental for the virus to enter host cells and initiate infection. (c) A schematic representation illustrates the use of atomic force microscopy (AFM) to probe the binding of SARS-CoV-2 to its target molecules. In this method, interactions between the virus and its receptor are monitored by AFM on model surfaces. The ACE2 receptor is immobilized on a surface, while the S1 subunit of the mutants is attached to the AFM tip. Source: [34].

**S2 Subunit,** It is responsible for the fusion of the viral and host cell membranes subsequent to receptor binding. It includes Fusion Peptide (FP) that helps insert the viral membrane into the host cell membrane and Heptad Repeat Regions (HR1 and HR2) that play a role in forming a structure necessary for membrane fusion [31].

### Mechanism of Virus Entry in Cell:

- 1. Attachment:** The S1 subunit (through the RBD or NTD) attaches the virus to the host cell's surface.
- 2. Proteolytic Cleavage:** Host cell proteases (enzymes that cut proteins) cleave the S protein

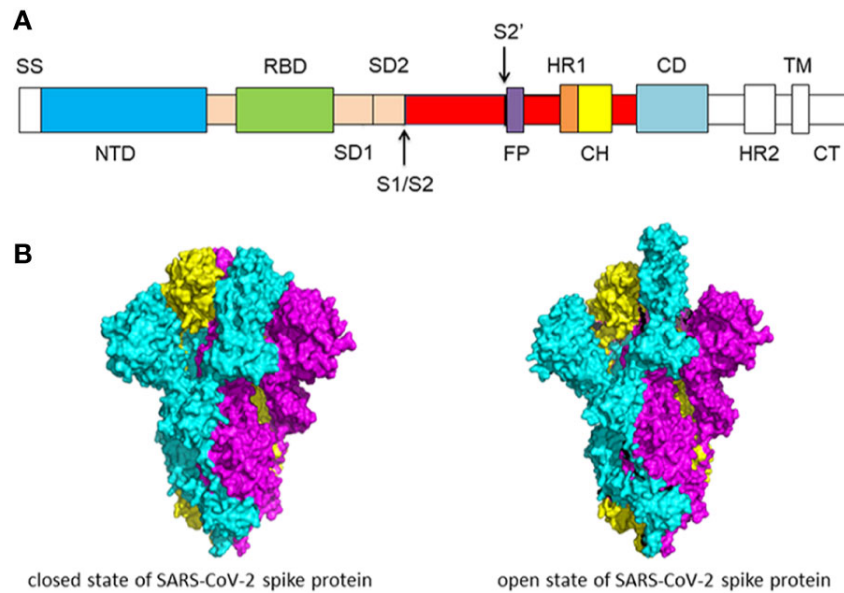


Figure 2.2: (A) A schematic representation of the SARS-CoV-2 spike protein highlights its various domains, each depicted in distinct colors. These domains play crucial roles in the protein's structure and function. (B) The cryo structure of the SARS-CoV-2 spike protein illustrates two conformational states: the closed state (left) and the open state (right) of the S glycoprotein. These states represent different configurations of the spike protein, which are essential for its interactions with host cell receptors and the fusion process during viral entry. Figure Source: [31].

at the S1/S2 boundary and another site termed S2'.

**3. Receptor Binding:** Cleavage at the S1/S2 boundary encourages the RBD in the S1 subunit to flip to its "up" conformation, enabling it to bind the host receptor (e.g., ACE2) with high affinity.

**4. Conformational Change:** Receptor binding triggers significant structural changes in the S2 subunit.

**5. Membrane Fusion:** The HR1 and HR2 regions of the S2 subunit (see figure 2.2) interact to form a six-helix bundle, bringing the viral and host cell membranes close together leading to their fusion. This enables the viral genetic material to enter the host cell.

The Wuhan variant (D614G) and the Omicron variant (B.1.1.529) of SARS-CoV-2, differ on both molecular and genomic levels, impacting their transmission and clinical characteristics. At the molecular level, the difference lies in the spike protein, responsible for viral entry into host cells. While both strains possess spike proteins, the Omicron variant boasts a significantly higher number of mutations, particularly within the receptor-binding domain (RBD) of the S1 subunit. These mutations enhance the Omicron variant's binding affinity to the human ACE2 receptor, potentially contributing to its increased transmissibility[19].

The Omicron variant appears to be generally more transmissible compared to the Wuhan strain, a phenomenon potentially linked to both its enhanced binding affinity to ACE2. However, the quantitative information like Dissociation rates, Energy barrier and etc. of these evolving virus and its variants is missing.

The SARS-CoV virus, responsible for COVID-19 is known to get entry into human cells through a specific receptor protein called Angiotensin-Converting Enzyme 2 (ACE2) [5]. ACE2 is a protein found on the surface of various human cells, particularly those in the lungs, heart, intestines, and kidneys.

Here, We study the biophysical properties of SARS-CoV-2 mutants binding to ACE2 receptors on immobilized surfaces using Force-Distance (FD) curve-based Atomic Force Microscopy (AFM). We analyze the thermodynamics of the interactions established in vitro, comparing the binding properties of Wuhan and Omicron mutant with the ACE-2 receptor.

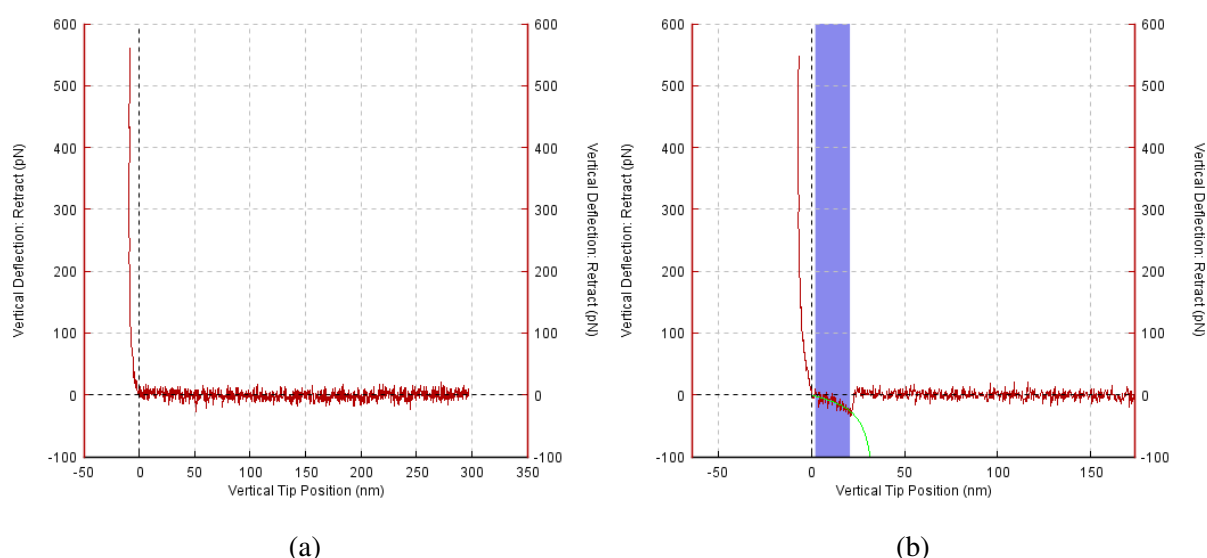


Figure 2.3: Figure(a) showing FD curve on gold surface with no interaction with ACE-2 (non adhesive contact) and Figure (b) showing FD curve showing deflection due to rupture of S1 and ACE-2 on surface with green curve is WLC fitting.

Single-molecule force probing techniques, such as Force-Displacement based AFM, measure the strength of a bond under an externally applied force. Using this approach of force probing we can get insights into the binding free-energy landscape.

According to the Bell–Evans model, developed by George Bell and M.G. Evans in 1970, provides a theoretical framework for understanding the relationship between the loading rate (LR) and the binding strength of a ligand-receptor bond under far-from-equilibrium conditions [34].

The model considers a two-state system: the unbound state (U) and the bound state (B) of the ligand-receptor complex. The transition between these states occurs through an energy barrier represented by the transition state (TS). The model assumes that the reaction coordinate, representing the progress of the reaction, is a linear function of the distance between the ligand and receptor. It further assumes that the force (F) applied to the system is proportional to the Loading Rate (LR). As the loading rate increases, the dissociation constant decreases, indicating a stronger binding affinity between the ligand and receptor.

Dynamic Force Spectroscopy (DFS) plots were obtained for both S1 subunits of Wuhan and Omicron variants with the immobilized ACE2 receptors on gold coverslip. In all cases, the unbinding force increases almost linearly with the logarithm of the LR upto a certain Loading Rates, as observed earlier for virus-receptor bonds. To know whether single- or multiple-bond rupture between S1 and ACE2 is taking place, every single F-D curve were analyzed through a varied ranges of Loading Rates, plotted as rupture force histograms and further fitted with multi peak Gaussian. The peak of these Gaussians are then plotted to fit the straight lines.

From the slope of the straight line fit, we can estimate the Distance to transition state ( $x_u$ ). The kinetic off-rate ( $k_{off}$ ) or dissociation rate can be obtained from the intercept of the straight line fit (at  $LR = 0$ ) [33].

## **2.2 METHODS**

### **2.2.1 GOLD COATING OF GLASS COVERSLIPS**

The following procedure is implemented to coat Gold on glass coverslips:

#### **Cleaning Procedure:**

The glass coverslips are subjected to a rigorous cleaning regimen utilizing Piranara Solutions. This initial step aimed to eliminate any organic contaminants and debris adhering to the coverslips' surfaces. Subsequently, the coverslips underwent sonication in a sequence of solvents to further cleanse and de-grease the surfaces with Acetone, Sonication in acetone is performed for a minimum of three cycles to dissolve any organic residues and contaminants followed by Methanol and finally with Milli Q Water, the coverslips were rinsed with Milli Q water to remove any remaining solvent residues and impurities.

Following the cleaning process, the coverslips were carefully affixed onto glass slides.

### **Thermal Vapor Deposition (TVD) of Gold:**

The prepared slides with affixed coverslips were introduced into the Thermal Vapor Deposition (TVD) chamber for the deposition of a thin layer of gold. The chamber is evacuated to a high vacuum level. Once the vacuum is achieved, a small gold piece is heated to its evaporation temperature, causing it to transition into a vapor phase. These vaporized gold atoms travel through the vacuum and condense onto the cooler surfaces of the coverslips, gradually forming a thin gold film. By precisely controlling the deposition parameters like time, temperature, and pressure, the thickness of around 50-60 nm and uniformity of the gold film is achieved.

### **2.2.2 PREPARATION OF ACE2-COATED GOLD SURFACES**

In the process of preparing the ACE2-coated surface, a series of steps are involved. Initially, the gold-coated coverslips were subjected to a thorough cleansing procedure involving treatment with UV and ozone for 15 minutes and washing from PBS buffer. Following this preparatory stage, a solution of linker mixture is put onto the coverslips. This linker solution consists of a mixture of ethanolamine and Nitrilotriacetic acid (NTA) ended molecules in a ratio of 95:5, and it was allowed to incubate overnight. These steps are shown in the figure.

The next phase involves the attachment of the ACE2 protein to the prepared surface. To achieve this, first ethylenediaminetetraacetic acid (EDTA) was put on the coverslip to eliminate the metal impurities in the solution, followed by the introduction of a nickel solution, this forms coordinate bonds with NTA ended linkers where the protein will attach and a subsequent buffer wash and EDTA of less concentration, this removes the excess nickel remained on the surface. prevent overcrowding, and promote the acquisition of clean data.

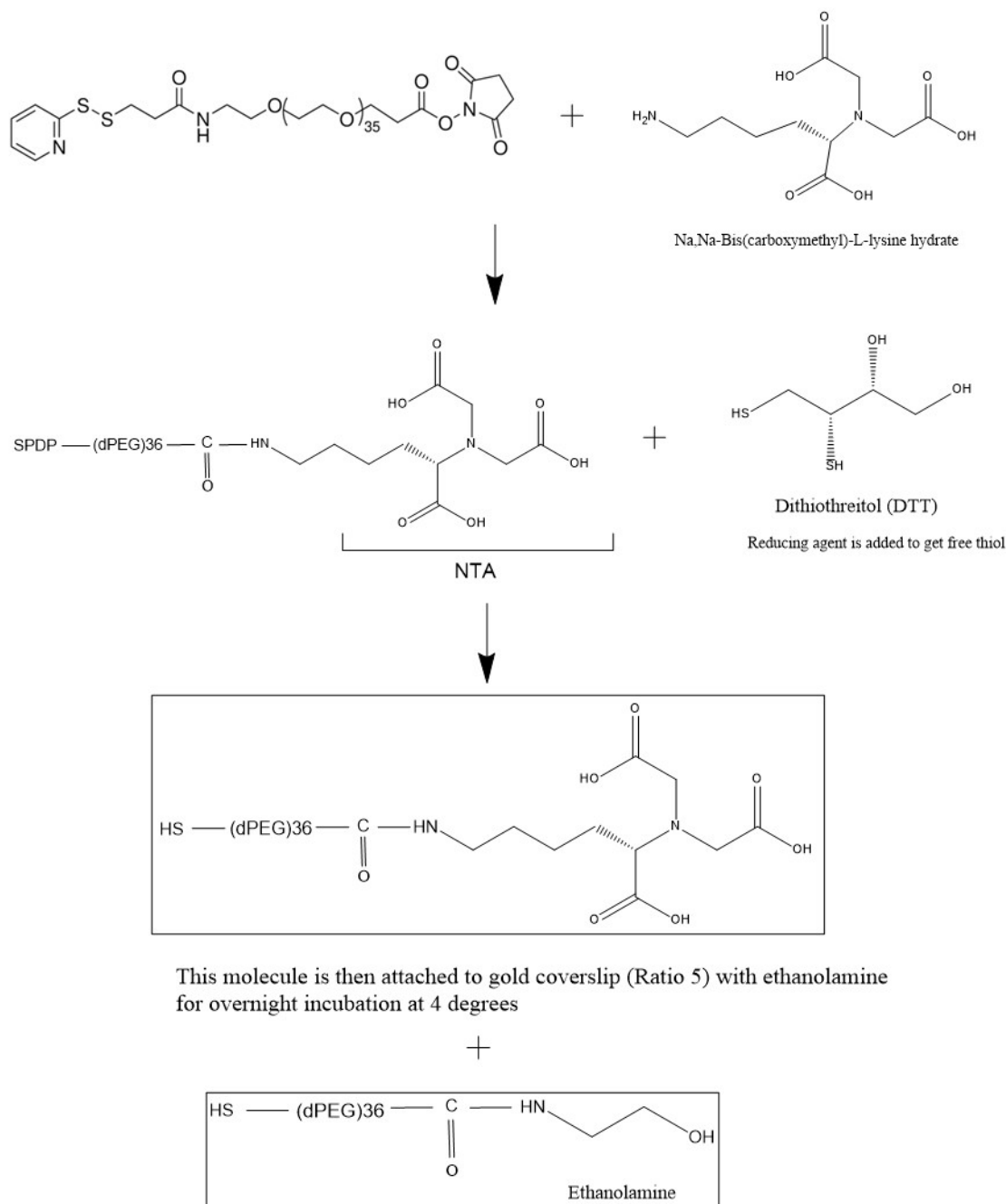
The final step is putting of 200 µg of ACE2 protein in PBS buffer onto the gold coverslip, which was already affixed with the NTA-linked linker. The NTA ended linker are efficiently bound with the ACE2 protein. The stepwise progression of these actions is also shown in the figure.

### **2.2.3 FUNCTIONALIZATION OF AFM TIPS**

To prepare the gold-coated cantilevers for functionalization, Initially, the cantilevers is also subjected to a thorough cleansing procedure involving treatment with UV and ozone for 15 minutes.

For the functionalization of the tips with the S1-subunit protein, Similar steps are followed till the addition of Nickel solution and washing with buffer. The only change is the protein 0.5 µg of the S1 protein, which was carefully applied to the cantilevers. These cantilevers are put on

Parafilm. Subsequently, the cantilevers were allowed to incubate in the protein solution for a duration of 1 hour. After this incubation period, the cantilevers were subjected to a washing procedure. To achieve this, 20  $\mu$ l of PBS buffer solution was gently introduced three times to ensure the thorough removal of excess protein solution from the cantilevers.



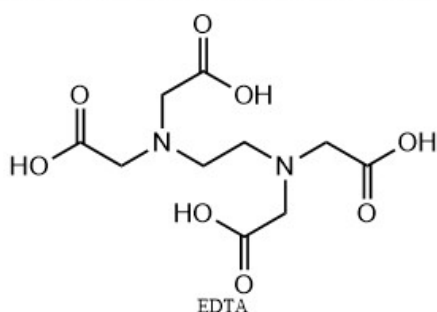
This molecule is also then attached to gold coverslip (Ratio 95)  
This is done to avoid over-crowding of protein

Figure 2.4: Functionalization steps to attach Linker molecule SPDP-(dPEG)<sub>36</sub>-NHS ester on Gold surface common for coverslip and cantilever

Now after completing overnight incubation with dPEF<sub>36</sub>-EENH<sub>2</sub> : dPEF<sub>36</sub>-NTA (95:5). We start the protein attaching protocol

Step 1: Three times wash with Buffer

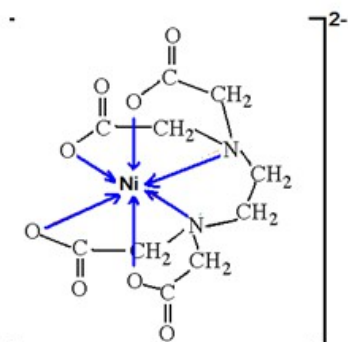
Step 2: Put 350 millimolar EDTA(Ethylenediaminetetraacetic) solution for 1 min



This binds with the excess linker

Step 3: Three times wash with Buffer

Step 4: Put NiSO<sub>4</sub> solution for 1 min



This Nickel forms complex with EDTA and helps in removing the excess growing

Step 5: Three times wash with Buffer

Step 6: Put 3 millimolar EDTA for 1 min

Step 7: Three times wash with Buffer

Step 8: Add human-ACE-2 protein solution and incubate for 1 hour at 4 degrees

Functionalization is completed at this step.

To functionalize the cantilever same steps are followed but the only change is the protein solution in this case we use spike CoV protein

Figure 2.5: Functionalization steps to attach protein after Linker molecule is attached on Gold surface common for coverslip and cantilever



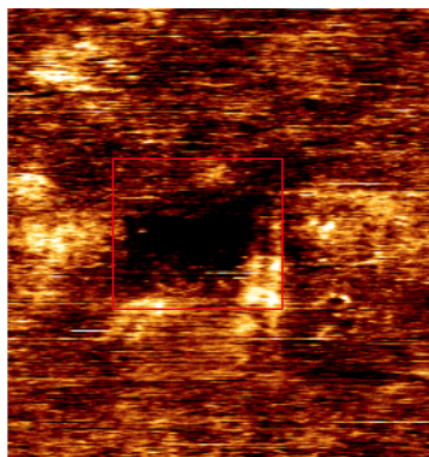
### 2.2.4 FD-BASED AFM ON MODEL SURFACES

Force Displacement based AFM on model surfaces was performed in PBS buffer at room temperature using functionalized gold-coated cantilevers with a spring constant of 0.05 N/m. On AFM, contact mode was used with areas of  $5 \times 5 \mu\text{m}$  scanned, z-length set to 500 nm, and set point force of 500 pN, with a resolution of  $32 \times 32$  pixels and a line frequency of 1 Hz.

Dynamic Force Spectroscopy analysis (using a constant approach speed of  $1 \mu\text{m/s}$  and variable retraction speeds of 0.1, 0.2, 1, 5, 10, and  $20 \mu\text{m/s}$ ) and kinetic on-rate estimation (measuring the BP for different hold times of 0, 50, 100, 150, 250, 500, and 1000 ms) were performed. All these changes in the retraction speeds are done to fit the Bell Evans model, as stated earlier in the introduction section.

## 2.3 RESULTS AND DISCUSSION

SARS-CoV-2 binding to ACE2 receptors is seen in FD curves (Fig. 2.3). FD curves are used to evaluate at the single-molecular level and the binding strength of the interaction are extracted from Bell- Evans Model. To replicate the cell-surface receptors in vitro, ACE2 receptors were functionalized onto gold surfaces to the free end to long polyethene glycol linkers (Functionalization steps explained in the Methods section). To confirm the deposition of layer of linker, the gold coverslip surfaces were scratched and then imaged by AFM, and the thickness of the functionalized layer was confirmed by the scratching experiment.



Redbox is scratched area

Figure 2.6: Figure showing AFM topography image of an ACE2 coated surface after scanning a  $1 \mu\text{m} \times 1 \mu\text{m}$  area at high forces (around 18 nN) and  $5 \mu\text{m} \times 5 \mu\text{m}$  imaged at very low force. We can clearly see a blacked out spot which confirms the attachment of Linker on the gold surface

Now, To study the interaction between the S1 subunit and the ACE2 receptors, we attached S1

subunit of mutants to the same free end of a long polyethene glycol (PEG)36 linker attached to the AFM tip cantilever and ACE-2 protein to the same linker attached on gold coverslip. (Also explained in Methods). To investigate the properties of the binding complex, that is S1 subunit of mutants and ACE2 receptor, force–distance (FD) curves were recorded by repeatedly approaching and retracting the functionalized cantilever from the ACE2 on Gold coverslip. Specific adhesion events were observed on 5-6 per cent of the retraction FD curves at rupture distances  $>25$  nm, which corresponds to the extension of the PEG linker. The histogram to these events is been shown in the Fig 2.6. This also confirms the PEG linkers attached on the both cantilever and the gold coated coverslips. [16]

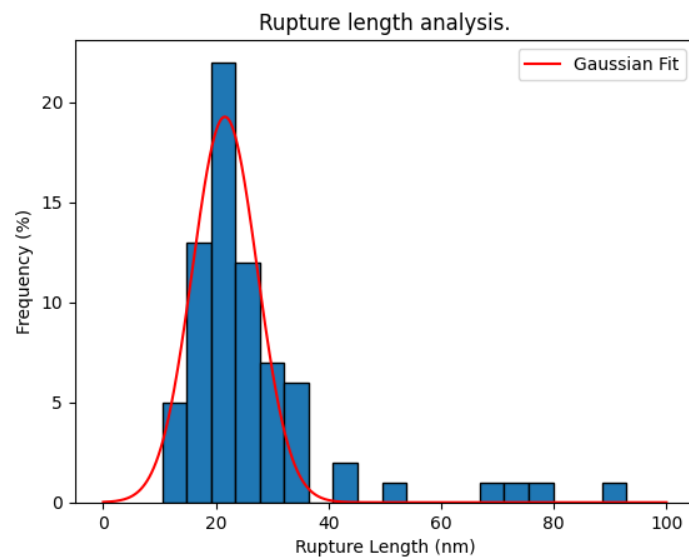


Figure 2.7: Histogram of rupture length for the S1-subunit and ACE2 interaction (N = 64 data points). Multipeak Gaussian fit reveals a maximum of the rupture force at  $28 \pm 9$  nm for the S1-ACE2 interaction

Force-Distance based Atomic Force Microscopy (AFM) is technique used to measure the strength of molecular bonds under the influence of an externally applied force. This method allows us to gain insights into the binding free-energy landscape of biomolecular interactions. According to the Bell–Evans model, when an external force is applied to a bond, it lowers the activation-energy barrier required for dissociation, thus reducing the lifetime of the ligand-receptor pair. Additionally, the model predicts that under conditions far from equilibrium, the binding strength of the ligand-receptor bond is directly proportional to the logarithm of the loading rate (LR). The loading rate describes the force applied to the bond over time. This relationship provides valuable information about the kinetics and thermodynamics of molecular binding events, facilitating a deeper understanding of biological processes such as ligand-receptor interactions and protein folding dynamics. By employing Force-Distance based AFM and incorporating the Bell–Evans model, we can elucidate the intricate mechanisms governing

molecular recognition and much more.

To explore the kinetics of the probed complex, Force-Distance (FD) curves were generated at various retraction rates as described in the methods section. Dynamic Force Spectroscopy (DFS) plots were then constructed for the S1 subunits of mutants, attached to a gold cantilever, interacting with immobilized ACE2 receptors on a gold coverslip. Notably, the unbinding force exhibited a linear increase in correlation with the logarithm of the Loading Rate (LR), aligning with the predictions of the Bell-Evans Model. To discern whether single or multiple bond ruptures occurred between the S1 subunit and ACE2, the FD curves were meticulously analyzed across discrete LR ranges. Subsequently, force histograms were constructed and fitted with multipeak Gaussian distributions. Through this approach, we aim to get the most probable unbinding force associated with each force peak, thereby determining the nature of the interactions, whether they involve single or multiple bonds.

The histograms will show that most probably only single interactions were taking place; thus, the Bell-Evans model [2] will be used to fit the data with straight line, enabling the interpretation of the binding of molecules as a two-state model, in which the bound state is separated from the unbound state only by a single energy barrier. From the slope of the fit, we aim to estimate the length scale of the energy barrier ( $x_u$ ), the kinetic off-rate ( $k_{off}$ ) or dissociation rate obtained from the intercept of the fit (at  $LR = 0$ ) [26].

From the slope of the fit, we estimated the length scale of the energy barrier ( $x_u$ ). We obtained very close values,  $x_u = 0.20$  nm and  $x_u = 0.35$  nm for both the Wuhan and Omicron variant respectively. The kinetic off-rate ( $k_{off}$ ) or dissociation rate is obtained from the intercept of the fit (at  $LR = 0$ ) yielding  $k_{off}$  values of  $K_{off} = 1.96$  per sec and  $K_{off} = 0.39$  per sec for the Wuhan and Omicron variant respectively.

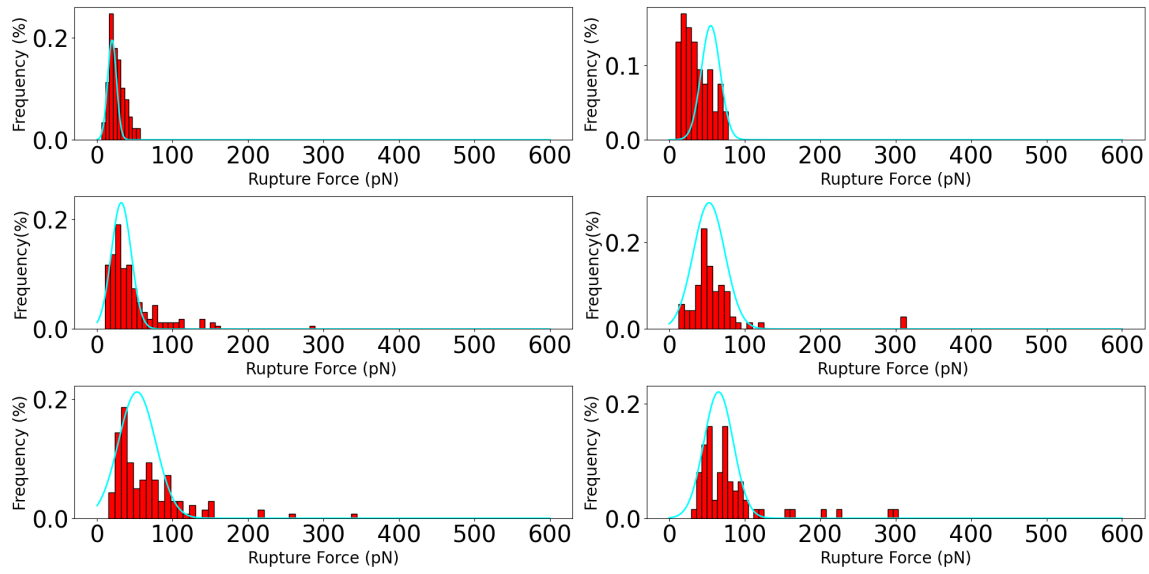


Figure 2.8: Figure showing the histograms of rupture forces for the 6 different set of loading rates and a gaussian is fitted of Wuhan variant. The maximum of the fit is used fit the straight line in the loading rate vs rupture force plots to get its intercept and slope to find the  $x_u$  and  $k_{off}$  respectively.

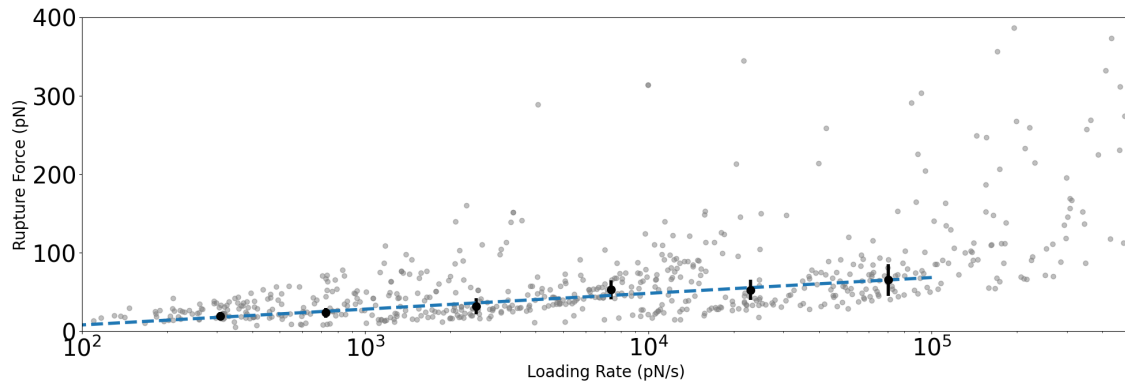


Figure 2.9: Figure showing the loading rate vs rupture force distribution for the Wuhan variant and the black dots are the maximum from the histograms plotted above and the grey dots are from the WLC fit from the FD curves taken at different retract speeds. The intercept and slope is extracted from the straight line which will be used to find the  $x_u$  and  $k_{off}$  of the interaction.

From the above data we can say that the length of energy barrier is more for the omicron variant and kinetic off rates are higher for Wuhan variant.

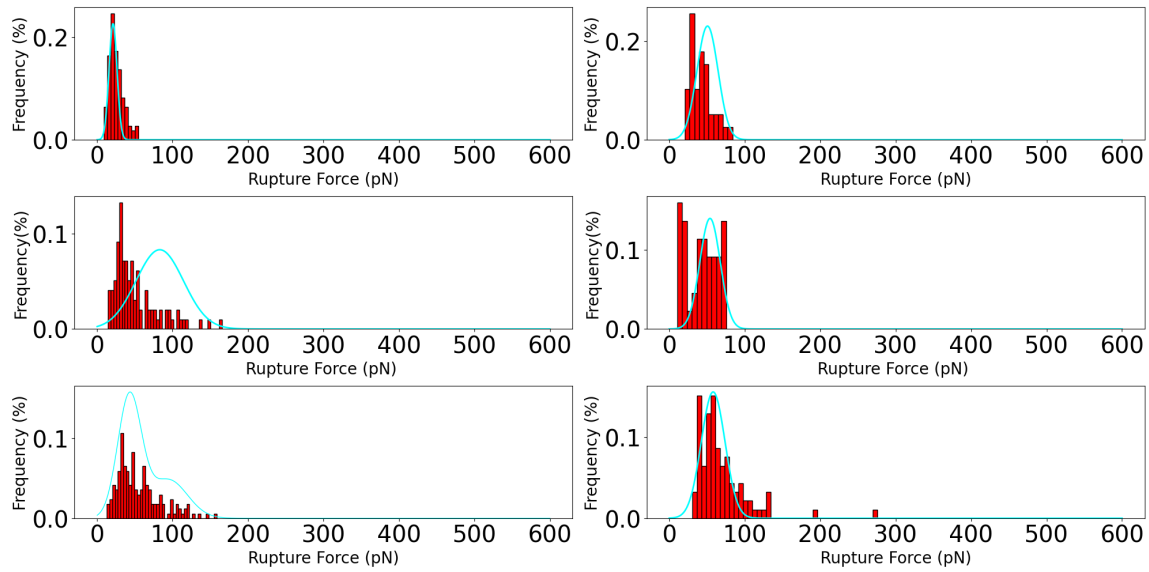


Figure 2.10: Figure showing the histograms of rupture forces for the 6 different set of loading rates and a gaussian is fitted of Omicron variant. The maximum of the fit is used fit the straight line in the loading rate vs rupture force plots to get its intercept and slope to find the  $x_u$  and  $k_{off}$  respectively.

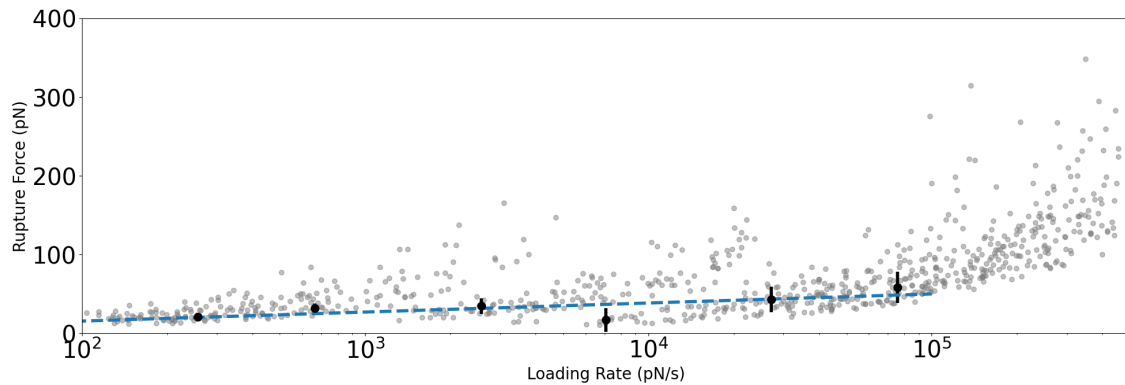


Figure 2.11: Figure showing the loading rate vs rupture force distribution for Omicron variant and the black dots are the maximum from the histograms plotted above and the grey dots are from the WLC fit from the FD curves taken at different retract speeds. The intercept and slope is extracted from the straight line which will be used to find the  $x_u$  and  $k_{off}$  of the interaction.

## 2.4 FUTURE PLANS

We want to do the same analysis for more mutants of CoV like, Single Mutant, Double Mutant, Triple Mutant, We also aim to use actual human cell lines from different tissue origins like the liver, lungs, and kidneys. This change will help us mimic the better and close to real conditions the virus encounters inside the human body. We will also follow the same analysis, including the Bell-Evans model explained in the result section for all the mutants. Finally, We also aim

to address how a mutation in the virus is affecting the binding with ACE2 on the model surface as well as cells, as explained earlier.

## **Chapter 3**

# **MEASURING VISCOELASTIC PROPERTIES OF L-CELLS LACKING CLATHRIN LIGHT CHAINS.**

### **3.1 INTRODUCTION**

Endocytosis is the fundamental cellular process by which cells bring substances from the extracellular environment into their interior. This vital mechanism plays a crucial role in various cellular functions, Cells absorb essential molecules like glucose, amino acids, and vitamins through endocytosis (Nutrient uptake), Binding of hormones and other signaling molecules to cell surface receptors triggers endocytosis, initiating intracellular signaling cascades ( Communication and signaling), Specialized immune cells called phagocytes engulf and eliminate pathogens and debris through endocytosis (Defense) Endocytosis also helps regulate the levels of proteins and lipids on the cell surface (Maintaining cell membrane composition). Endocytosis retrieves worn-out or unwanted molecules from the cell surface for degradation or reuse (Recycling and degradation) [12].

There are different forms of endocytosis, each with unique characteristics and functions some of them are; Phagocytosis (cell eating), This specialized form involves engulfing large particles, like bacteria, dead cells, or debris, by extending pseudopodia (cell extensions) and forming a phagosome (digestive vacuole) around them providing a defense mechanism for immune cells like macrophages and neutrophils, eliminating harmful agents and cellular debris.

#### **Pinocytosis (cell drinking)**

A more general process where the cell membrane invaginates and pinches off small vesicles containing fluids and solutes from the surrounding environment.

#### **Caveolae-mediated endocytosis**

It utilizes caveolae, small flask-shaped invaginations of the plasma membrane, to internalize specific molecules and lipids. Caveolae are enriched in cholesterol and associated proteins, this is involved in signal transduction, cholesterol uptake, and regulating cell proliferation and

differentiation.

### **Clathrin-mediated endocytosis (CME)**

CME is a highly regulated and selective process responsible for internalizing specific cargo molecules and their associated receptors from the cell surface. It plays a critical role in various cellular functions, including nutrient uptake, receptor recycling, and signal transduction.

Clathrin-mediated endocytosis utilizes a protein coat called clathrin to form coated pits on the cell surface. These pits then invaginate and bud off as clathrin-coated vesicles, specifically containing the targeted cargo and its receptors. Unlike other endocytosis forms, CME is highly selective, ensuring only specific molecules are internalized. CME involves several key steps such as Cargo Selection, adaptor proteins recognize specific signals on cargo molecules and receptors, initiating the assembly process. Clathrin Coat Formation, clathrin triskelia (three-pronged structures) assemble around the adaptor-cargo complex, forming a latticework coat. Pit Formation, the clathrin coat induces membrane curvature, creating a shallow pit on the cell surface etc. CME is a vital mechanism for maintaining cellular homeostasis and responding to external stimuli. Its selective nature allows for precise control over the internalization of specific molecules, ensuring proper cell signaling and nutrient uptake. Dysregulation of CME is linked to various diseases, highlighting its significance in human health [10].

Clathrin itself is a complex molecule composed of heavy and light chains. Heavy Chains form the triskelia structure, the building block of the clathrin coat, containing multiple domains responsible for assembly, interaction with cargo adaptors, and membrane binding. Modifications on the heavy chain can regulate clathrin function and cargo selection. Light Chain In invertebrates is encoded by a single gene. However, as a result of local gene duplication, higher eukaryotes have two light chains, CLCa and CLCb encoded by the genes Clta and Cltb, respectively.

Light chains are attached to the heavy chain and influence its interactions with other proteins. It also plays a role in stabilizing the clathrin lattice and regulating uncoating. Variations in the clathrin heavy and light chains alter the biophysical properties of the clathrin lattice, in turn affecting trafficking of receptors and thereby several physiological functions of the cell. The heavy chain is essential for triskelion assembly and for all clathrin-dependent endocytic events, with a number of excellent reviews highlighting the function of this protein [10]. In contrast, the studies of the clathrin light chains remains relatively under-explored.

L cells, derived from the areolar adipose tissue of a 100-day-old male mouse. Areolar tissue,



classified as loose connective tissue, providing mechanical support and versatility. In contrast, adipose tissue, commonly referred to as fat tissue, comprises specialized connective tissue mainly composed of adipocytes (fat cells). It serves as a crucial energy repository for the body, storing surplus energy in the form of triglycerides [29].

The objective of this experiment is to find out the mechanical properties of L cells and their corresponding clathrin light chain knockout variants, namely *clta*, *cltb*, and the combined knockout of both subunits *cltab* using Atomic Force Microscopy (AFM) and understanding how the absence of clathrin light chain subunits namely *clta*, *cltb* and *cltab* influences the mechanical properties of these cells, with an emphasis on their Elasticity (The ability of a material to deform and return to its original shape after the applied force is removed) and Viscoelastic parameters. This investigation will provide valuable insights into the role of clathrin light chain in the mechanical behavior of cells and its impact on essential cellular processes, expanding our understanding of cell biology and the consequences of these knock-outs in clathrin-mediated endocytosis and various physiological contexts.

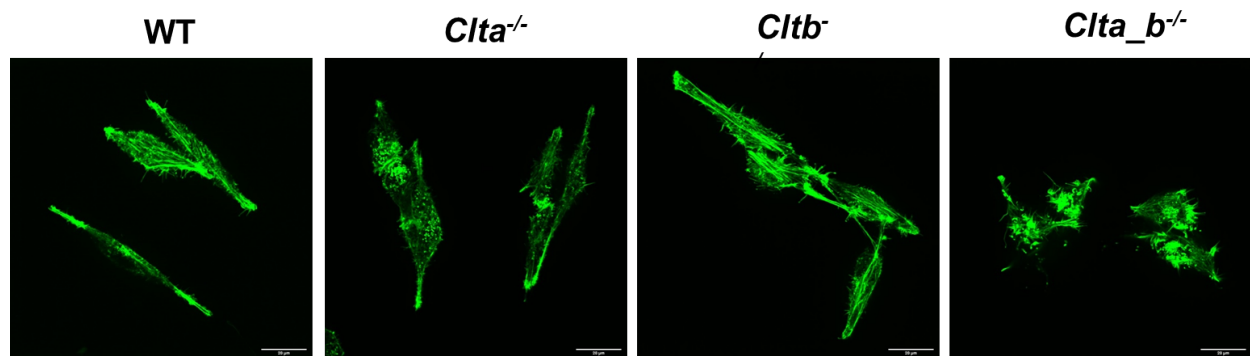


Figure 3.1: Clathrin light chain a and b knockout was made in L cells with the help of CRISPR/Cas9. Here, green is phalloidin, which stains F actin. Actin patches are more prominent in clathrin light chain a and ab double knockouts than in the wild type. Image Credit: Surya Bansi, Dr Deepa's Lab, NCCS

In this experiment, the mechanical properties of over 20 cells from each cell phenotype were examined under the AFM using a small 5-micron diameter glass bead glued on the cantilever using "lift off" method explained in Methods section. To determine the elasticity of these cells, an analysis method known as the Hertz fit was used, which is accessible through the JPK data processing software. The Hertz fit is a mathematical model used to estimate the Young Modulus, a fundamental parameter for characterizing the elasticity of materials.

The Hertz fit model is based on the Hertz contact mechanics theory, which describes the de-

formation of an elastic material under the influence of a conical or spherical indenter(in this case). This theory provides a mathematical framework to estimate the Young Modulus (E), which characterizes the material's elasticity. The Hertz fit is a tool for determining the Young Modulus of materials, including biological samples like cells. The fundamental equation that underlies the Hertz fit is:

$$F = \frac{2}{3} \frac{E}{1 - \nu^2} \frac{R^{1/2}}{d^{3/2}} \delta^{3/2}$$

Where:

$F$  : Applied Force

$E$  : Young's Modulus

$\nu$  : Poisson's Ratio (typically assumed as 0.5 for biological samples)

$R$  : Radius of the Indenter Tip

$d$  : Indentation Depth

$\delta$  : Tip-Sample Separation

The Hertz fit method involves curve fitting to the force-displacement data collected during the nano-indentation experiments. This analysis helps in characterizing the mechanical response of the cells, specifically in relation to their deformation under an applied force.

The Hertz model assumes a purely elastic nature of the sample, while in reality most biological samples are viscoelastic. Viscoelasticity is a combination of viscous (flow-like) and elastic (solid-like) properties, plays a crucial role in understanding the dynamic response of biological materials under mechanical stress. It is revealed in a clear hysteresis between the approach and retraction parts of curves.

Here, we have used a new method developed by Prof Arvind Raman and group [13] to extract viscoelastic properties of soft samples like cells and hydrogels directly from standard AFM F-Z curves. This method is based on the theoretical model developed by Ting for the problem of the indentation of a linear viscoelastic half-space by a rigid axisymmetric indenter for arbitrary load history. By combining Ting's model with pertinent numerical procedures, the group was able to process data from both the approach and retraction phases of the experimental F-Z curves to get the viscoelasticity and parameters. The key advantage of this method lies in its robustness, as it doesn't need any alterations to the experimental design. Moreover, it is compatible with traditional AFM rheology techniques.

The viscoelastic behaviour of soft materials can often be described using the power-law rheology equation, which can be expressed as:

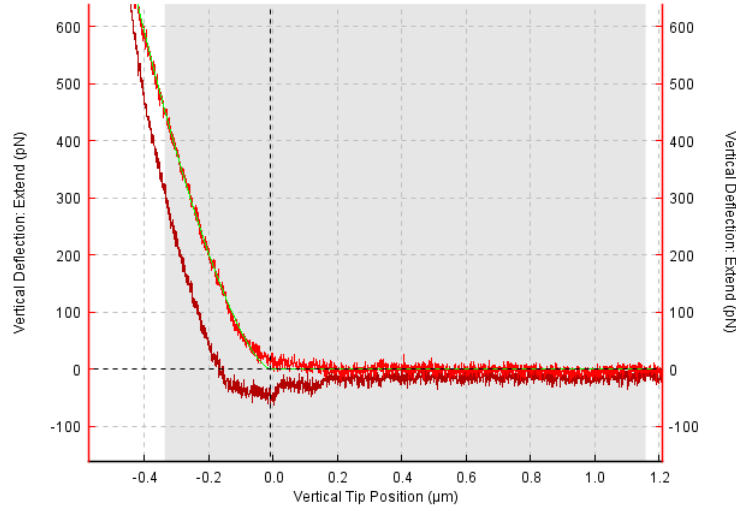


Figure 3.2: Figure showing a plot of Tip position vs Deflection) with a Approach (Light Red) and Retract (Dark Red) curve on cell with the green curve is Hertz Fit. The hysteresis between approach and retract part is used to calculate the viscoelastic Parameters.

$$G(t) = G_0 \cdot t^\alpha$$

Here:

- $G(t)$  represents the time-dependent shear modulus or viscoelastic response at time  $t$ .
- $G_0$  is the instantaneous or short-time shear modulus.
- $\alpha$  is the power-law exponent that characterizes the viscoelastic behaviour of the material.

The power-law exponent ( $\alpha$ ) provides insight into the type of viscoelastic behaviour exhibited by the material. Different values of  $\alpha$  correspond to different rheological behaviours. For instance:

- $\alpha = 0$  indicates a purely elastic (Hookean) behaviour.
- $0 < \alpha < 1$  signifies a viscoelastic, yet predominantly elastic response.
- $\alpha = 1$  represents a linear viscoelastic response.
- $\alpha > 1$  indicates a predominantly viscous behavior.

This equation with the parameter  $\alpha$  is a valuable tool for characterizing the viscoelastic properties of materials, capturing the time-dependent response, and elucidating the relative contributions of elasticity and viscosity.

This extension of our analysis will provide a more in-depth perspective on how the absence of clathrin-light chain subunits influences not only the cells' elasticity but also their viscoelastic response. By doing so, we can uncover additional layers of information about the mechanical behaviour of these cells, further advancing our comprehension of the impact of clathrin-

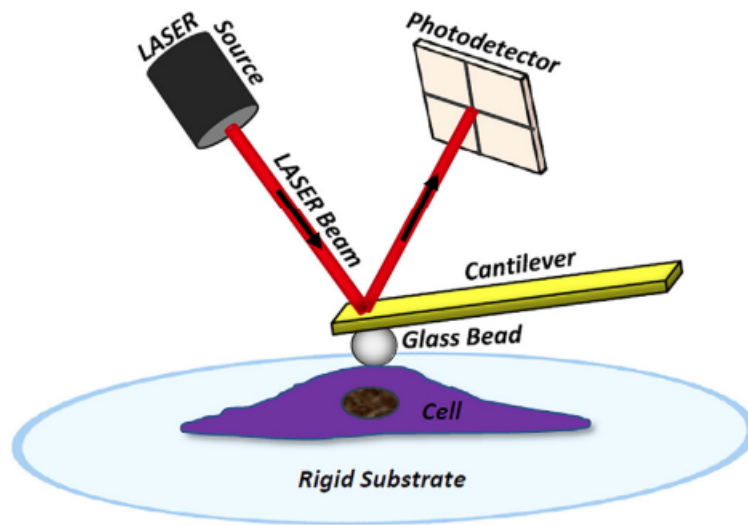


Figure 3.3: Fig. shows The tip, with a bead glued on it, interacts with the sample, and the interaction forces cause the microcantilever to deflect (bend) and the deflection on cantilever is read by the photodetector Source: [28].

mediated endocytosis on cellular biomechanics.

## 3.2 METHODS AND MATERIALS

### 3.2.1 BEAD ATTACHMENT

In the nanoindentation experiments conducted on single cells, we glued a glass bead with a 5  $\mu\text{m}$  diameter attached to gold cantilevers using the lift-off method that is:

Step 1: Carefully drop-cast a small amount of the diluted glass-bead solution in methanol onto the clean glass coverslip and allow the solution to dry completely for at least 1 hour. This ensures the methanol evaporates and the beads are firmly attached to the coverslip (See Fig 3.3 A).

Step 2: Measure and mix the Araldite Klear epoxy resin and hardener in a 1:0.8 ratio. Use a clean and dry coverslip for mixing and use a sharp needle/toothpick to pick up a tiny drop of the prepared epoxy mixture and carefully place a few small drops of the epoxy mixture onto the same coverslip, spaced slightly apart from the dried beads.

Step 3: Using the AFM carefully maneuver the free end of the tipless cantilever to the edge of one of the epoxy drops on the coverslip and approach the cantilever on the glue and then gently retract the cantilever away from the epoxy drop (See Fig 3.3 C).

Step 4: Move the cantilever closer to the area on the coverslip where the dried glass beads are located. Gently tap the cantilever on the coverslip a couple of times. This helps remove any excess epoxy and ensure a thin layer remains on the tip for optimal bead attachment. Using the AFM's auto-approach mechanism, carefully approach the cantilever towards a single, clean glass bead (See Fig 3.3 D).

Step 5: Keep the cantilever in contact with the chosen bead for at least 30 minutes under feedback control (force monitoring). This allows sufficient time for the epoxy to cure and form a strong bond between the bead and the cantilever tip.

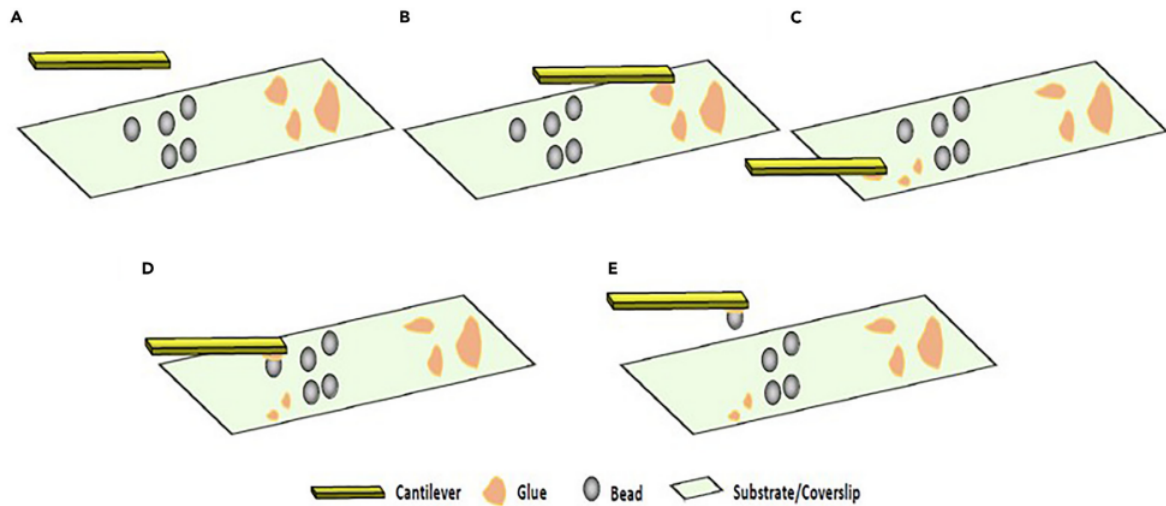


Figure 3.4: Fig. shows stepwise protocol to attach bead on cantilever as explain above. Source: [28].

### 3.2.2 NANOINDENTATION EXPERIMENTS

Prior to each experiment, two crucial parameters were determined: the photodetector sensitivity and the cantilever force constant.

The detection sensitivity, expressed in nanometers per volt (nm/V), is established by analyzing the slope of the approach curve, particularly in the region where the cantilever made deep contact with the glass slide. This provided us with a reliable measure of the sensitivity needed for precise measurements. Simultaneously, the force constant of the cantilever was ascertained using the thermal tuning method explained in chapter 1, which is a feature available in the software. Typically, cantilevers with a force constant of about 0.1 N/m are used for experiments. The experiments involving the approach and retract process is executed on individual live cells.

This involved maintaining a constant approach and retract speeds of 2  $\mu\text{m/s}$  over an area of 1 x 1  $\mu\text{m}^2$  onto cells. The data was sampled on a 7 x 7 grid. This detailed data acquisition strategy allowed us to gather the mechanical properties of the single cells under investigation.

### **3.2.3 DATA ANALYSIS**

For the Elasticity analysis of the acquired data, the Hertz fit was applied. This analysis was performed using specialized JPK data processing software.

For the Viscoelasticity analysis the MATLAB code written by Prof Arvind Raman group and modified by Dr. Shatruhan Singh Rajput is used.

### **3.2.4 SOURCING OF L CELLS**

The project is in collaboration with Dr. Deepa Subramanyam, National Centre for Cell Science (NCCS), Pune. The cells are taken to us by Surya Bansi and clathrin light chain knockouts were prepared by Mahak Tiwari, both from Dr. Deep's Lab, NCCS.

## **3.3 RESULTS AND DISCUSSION**

Previous work has demonstrated that a loss of CME in embryonic stem cells results in an altered organization of the actin cytoskeleton and an increased cellular stiffness [23]. The branched actin network is known to generate force required in many cellular processes including endocytosis, with alterations in this network directly limiting force transmission [20] [25].

The mechanical response by measuring  $\alpha$  and Elasticity, observed in the absence of clathrin light chains also appears to be linked to the altered state of actin organization in L cells since we have observed stiffness drop upon knocking out clathrin light chains.

In L cells the resulting Young Modulus in the absence of clathrin light chain subunits affects the mechanical properties of the cells.

The obtained Young Modulus values for each cell type are as follows:

1. WT:  $563.27 \pm 181.79 \text{ N/m}^2$
2. Clta:  $386.77 \pm 119.19 \text{ N/m}^2$
3. Cltb:  $385.47 \pm 119.91 \text{ N/m}^2$
4. Cltab:  $500.59 \pm 169.03 \text{ N/m}^2$

In the absence of clathrin light chains the measured  $\alpha$  values are plotted in Figure 3.6 (b).

The mechanical response by measuring  $\alpha$ , observed in the absence of clathrin light chains also appears to be linked to the altered state of actin organization in L cells. When the clathrin a and clathrin b are knocked out the stiffness is dropped by around 30 percentage but when both a and b are knockouts the stiffness again increases and now the drop is only around 10 percent. This confirms from the elasticity, previous work and image analysis that clathrin light chains altered state of actin organization in L cells.

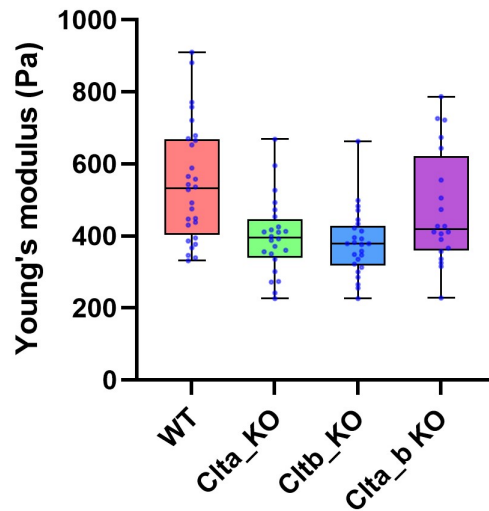


Figure 3.5: Figure showing Box plot of Young's Modulus comparison of WT, Clta, Cltb and Cltab

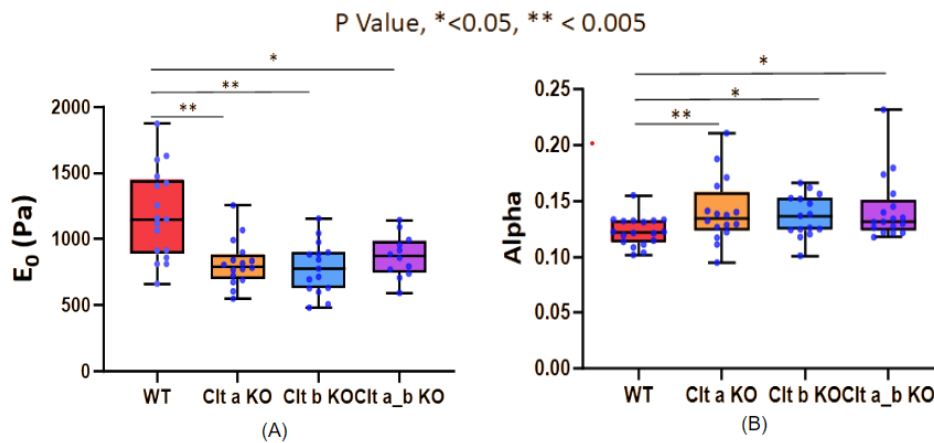


Figure 3.6: Figure (A) showing box plot of  $E_0$  values of L cells and corresponding clathrin light chain knockout phenotypes and Figure (B) showing box plot of  $\alpha$  values of L cells and corresponding clathrin light chain knockout phenotypes.

## **Chapter 4**

# **QUANTITATIVE EVALUATION OF COLLAGEN ORGANISATION AND ITS REGULATION BY MOUSE FIBROBLASTS IN 3D HYDROGELS USING AFM**

### **4.1 INTRODUCTION**

Mechanotransduction is a fundamental process through which cells perceive, interpret, and respond to mechanical cues from their surrounding microenvironment. Central to this process is the ExtraCellular Matrix (ECM), a complex network of proteins and carbohydrates that provides structural support to tissues and organs. Cells are not passive entities within this matrix; rather, they actively interact with and respond to mechanical stimuli, which play crucial roles in various physiological and pathological processes, including development, tissue homeostasis, wound healing, and disease progression [27].

At the heart of mechanotransduction lies the ability of cells to convert mechanical forces into biochemical signals, which then trigger a cascade of cellular responses. This process involves a sophisticated interplay between cell surface receptors, cytoskeletal elements, and intracellular signaling molecules. Through these interactions, cells are able to sense changes in mechanical tension, compression, shear stress, and substrate stiffness, among other mechanical cues, and translate them into specific biological outcomes.

Mechanosensors play a pivotal role in the process of mechanotransduction, serving as specialized molecules or complexes within the cell that act as the first responders to mechanical cues, detecting and transducing them into biochemical signals. These sensors are diverse and dynamic, with various components finely tuned to perceive and relay mechanical information to the cellular machinery [7]. Among the prominent mechanosensors are integrins, focal adhesions, cadherins, and caveolae, each contributing uniquely to the intricate process of mechanotransduction.

Integrins stand out as key players in mechanosensing due to their dual role as physical linkages



between the ECM and the cytoskeleton and as signaling hubs that translate mechanical stimuli into biochemical signals [24]. These transmembrane proteins undergo conformational changes in response to forces exerted on the cell surface, leading to the activation of downstream signaling pathways. By mediating cell-ECM interactions, integrins play critical roles in cell adhesion, migration, and signaling, thereby influencing various physiological and pathological processes.

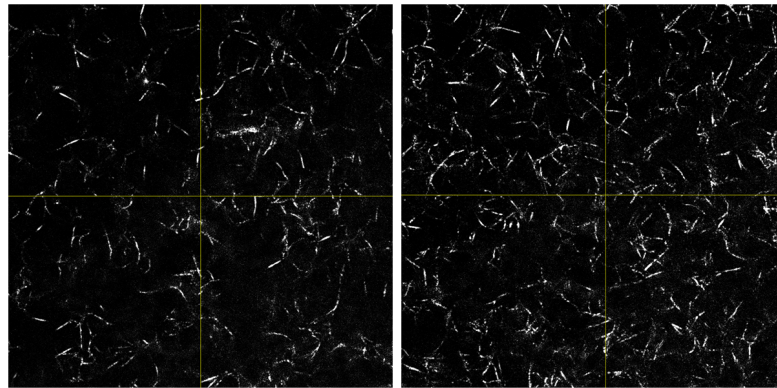
Cadherins, transmembrane proteins that mediate cell-cell adhesion through homophilic interactions, also contribute to mechanotransduction by sensing and responding to mechanical forces. In addition to their adhesive functions, cadherins are capable of transmitting mechanical signals across cell-cell junctions, influencing cell behavior and tissue morphogenesis. Through conformational changes induced by mechanical tension, cadherins can modulate cell-cell adhesion strength and signaling, thereby affecting tissue architecture and function [21].

Caveolae are invaginations of the plasma membrane enriched in cholesterol and caveolin proteins, and have emerged as intriguing candidates for mediating mechanotransduction. The involvement of caveolae in mechanotransduction is multifaceted [8]. Firstly, caveolae are enriched in various signaling molecules, including G-proteins, kinases, and ion channels, making them ideal platforms for signal transduction. Mechanical forces acting on the cell membrane can induce changes in caveolar shape and dynamics, leading to the activation or modulation of signaling pathways associated with caveolae.

Additionally, caveolae have been implicated in the regulation of membrane tension and lipid composition, both of which can influence mechanotransduction processes. Changes in membrane tension can impact the activity of mechanosensitive ion channels and receptors, thereby modulating cellular responses to mechanical stimuli. By modulating the organization and activity of signaling molecules, caveolae may play crucial roles in fine-tuning cellular responses to mechanical stimuli, thereby contributing to tissue homeostasis and function but the effect of Caveolin in organization of the microenvironment near the cell and the mechanisms by which caveolae participate in mechanotransduction are missing.

3D Collagen hydrogels with embedded with Wild-Type Mouse Fibroblast cells (WTMEFs) and Caveolin-1 Null Mouse fibroblasts (Cav-1<sup>-/-</sup> MEFs) serve as an excellent model system for studying cell-matrix interactions in three dimensions, mimicking the native ExtraCellular Matrix (ECM) environment more closely than traditional two-dimensional cell culture systems [32]. Additionally, by manipulating the collagen concentration in the hydrogels, We can modulate the density and organization of the ECM. The inclusion of WTMEFs in the hydrogels allows for the investigation of cell-mediated remodeling of the ECM and its impact on mechan-

otransduction pathways. By embedding fibroblasts in collagen hydrogels, We can observe how changes in collagen concentration alter the organization and alignment of collagen fibers near the cells, influencing their mechanical microenvironment.



(a) Fig. shows Collagen gel with the concentration of 1.0 mg/ml (b) Fig. shows Collagen gel with the concentration of 1.5 mg/ml

Figure 4.1: 3D Collagen hydrogel – Reflectance Imaging, Difference in branch number with changing the concentration of collagen. Figure Credits: Debasmita Mazumdar from Dr Nagraj Lab

The primary focus is to study the role of Caveolin in modulating the microenvironment near the cell and its involvement in mechanotransduction. Atomic Force Microscopy is used to quantify the mechanical properties of MEFs, its phenotypes and the hydrogels.

Latrunculin-A (Lat A) is a potent inhibitor of actin polymerization, which disrupts the organization of the actin cytoskeleton [15]. By treating WT MEFs and Cav-1 Null MEFs with Latrunculin-A, We can investigate the role of actin cytoskeleton dynamics in cell-matrix interactions and mechanotransduction and influencing collagen organization, allowing for an exploration of different mechanical properties. In both WT MEFs, and Cav-1 Null MEFs, which lack Caveolin-1, Latrunculin-A treatment would lead to actin depolymerization, resulting in alterations in cell morphology, and significant drop in elasticity.

Rock Inhibitor blocks the activity of Rho-associated protein kinase (ROCK), a key downstream effector of Rho GTPase involved in actomyosin contractility and cytoskeletal dynamics [22]. Treating WT MEFs and Cav-1 Null MEFs with Rock Inhibitor allows us to examine the effect of the Rho/ROCK signaling pathway in mechanotransduction and influence in collagen organization. In MEFs, Rock Inhibitor treatment would lead to relaxation of the actomyosin cytoskeleton, decreased cell contractility, and potentially altered responses to mechanical stimuli. By comparing the responses of WT and Cav-1 Null MEFs to Rock Inhibitor treatment,

we can assess the interplay of the Rho/ROCK pathway in mechanotransduction and cellular responses to mechanical cues [14].

## **4.2 METHODS**

### **4.2.1 SOURCING OF CELLS, PHENOTYPE AND GEL**

The cell types WT MEFs, Cav-1 Null MEFs, Lat A treated WT MEFs and Cav-1 Null MEFs, Rock Inhibitor WT MEFs and Cav-1 Nulls MEFs, Poly L Lysine coated and Collagen gel of both concentrations are prepared by Debasmita at Dr. Nagraj's Cell Adhesion Lab IISER Pune.

### **4.2.2 AFM INVESTIGATION OF COLLAGEN GEL**

The initial AFM investigation of pure collagen gels at different concentrations (1.0 mg/ml and 1.5 mg/ml) is done on a time scale of 15 minutes to 4 hours. I have used a 100-micron glass bead glued on the lower side of the tipless soft gold-plated cantilever with a spring constant of around 0.03 N/m. Force-distance curves are taken with a very low indentation force of 0.2nN. Young's Modulus is determined by the Hertz model fitted to the retracted part of curves.

### **4.2.3 AFM INVESTIGATION OF MEFS CELLS**

To investigate the stiffness of cells, I have used a smaller 2.5-micron (radius) glass bead glued on the tipless cantilever. The cells were probed with a maximum of 0.5nN indentation force at random measurement points along the cell surface on the centre, for four different sets and at least 20 cells of each type. Force-distance curves were analysed by fitting the Hertz model.

### **4.2.4 ANALYSIS OF ELASTICITY DATA**

The Elasticity of Cells and Gels were analysed by JPK data processing software using Hertz Fit. The curves were fitted only till 0.5nN for the case of cells and 0.2nN for gels. The curves were fitted this much to capture the most reliable and linear portion of the force-indentation curve relevant to understanding the elasticity of these materials. Analyzing data beyond these points might introduce inaccuracies due to the limitations of the model.

## **4.3 RESULTS AND DISCUSSION**

The data of stiffness of WT MEFs, Cav 1 Nulls and both treated with Lat A and Rock Inhibitor is extracted using Nanoindentation experiments and analysed using Hertz fit. The experiment is extended for different concentration of Lat A (Figure 4.3) and Rock Inhibitor (Figure 4.4). Nanoindentation experiments using Atomic Force Microscopy (AFM) were conducted on all cell phenotypes to quantify their stiffness (elasticity). This technique involves indenting the

single cell surface with a calibrated AFM tip and recording the force-displacement curve.

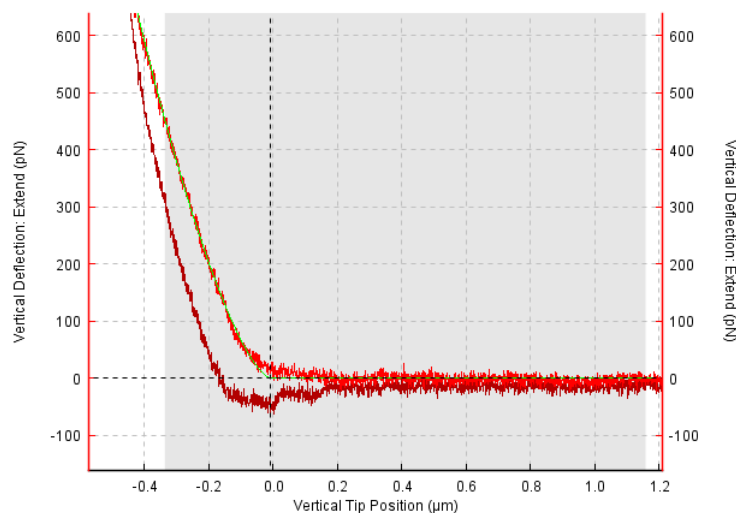


Figure 4.2: Figure showing a plot of Tip position vs Deflection with a Approach (Light Red) and Retract (Dark Red) curve on single cell.

The acquired data was then analyzed using the Hertz model, this analysis allowed us to extract the stiffness values for WT MEFs and Cav-1 Nulls, providing quantitative comparisons of their mechanical properties.

Stiffness measurements were performed on both WT MEFs and Cav-1 Nulls following treatment with varying concentrations of Latrunculin A and Rock Inhibitor. The treatments with Latrunculin A and a ROCK inhibitor are known to target actin filament dynamics and actomyosin contractility, respectively, both of which can influence cell mechanics.. This allowed us to identify the specific concentration at which the stiffness of both cell types that is WT and Cav 1 Nulls becomes comparable. This information allows us to compare the change in microenvironment with these embedded cells with no change in their stiffness.

The results, presented in Figure 4.3 and 4.4, demonstrate the differences in stiffness between WT MEFs, Cav-1 Nulls and upon Latrunculin A treatment. Similar experiments were conducted with a ROCK inhibitor, and the results are depicted in Figure 4.4. These stiffness data will be used to know the change in branch number and branch junctions to know the change in micro-environment upon putting these cells inside the collagen matrix of different concentrations.

Cells within the 3D matrix adopt a more rounded shape unlike the flattened and spread-ed morphology observed on coverslips. Based on the possibility that the stiffness differences might diminish in rounded cells, we applied poly-L-lysine coated coverslips to prevent spreading.

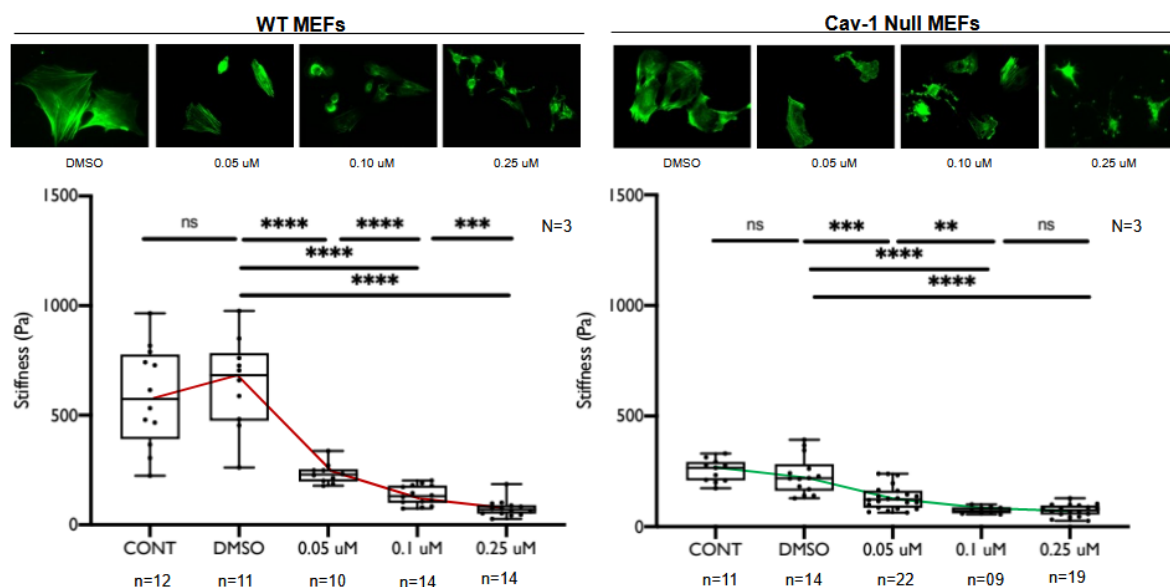


Figure 4.3: Figure shows two plots left is the comparison of stiffness of WT MEFs with 3 different concentrations of Lat A along with there reflectant images on top of the plots similarly on right is the comparison of stiffness of Cav Null MEFs with 3 different concentrations of Lat A along with there reflectant images on top of the plots. Image Credits: Debasmita Mazumdar from Dr Nagraj Lab

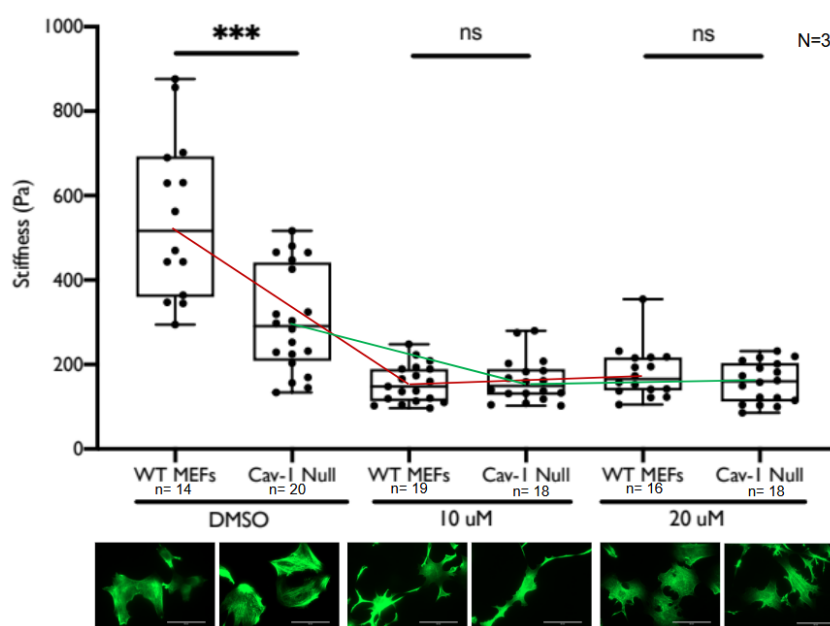
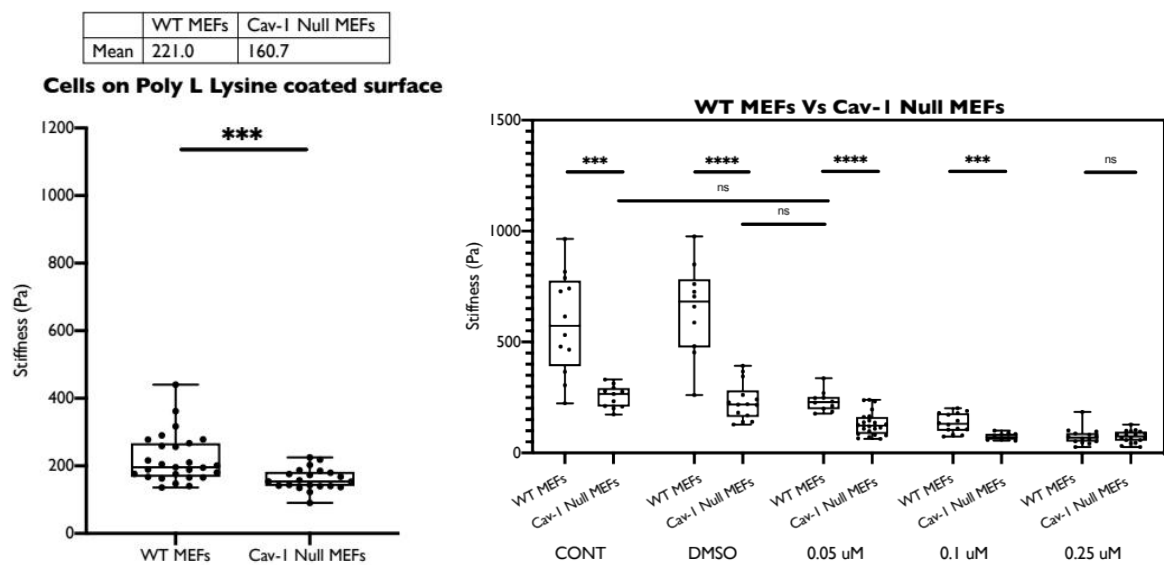


Figure 4.4: Figure stiffness change on adding Rock Inhibitor of two different concentration.

This approach ensured the cells remained round, mimicking their morphology within the 3D matrix. Stiffness measurements were performed on these round cells, and the results are shown in Figure 4.5 (a). Notably, the data reveals that the stiffness difference is still there between WT MEFs and Cav-1 Nulls, even in their rounded state.



(a) Stiffness difference with Poly L ly- (b) Figure shows a plot with stiffness comparison of WT and Cav  
sine coated coverslip Null

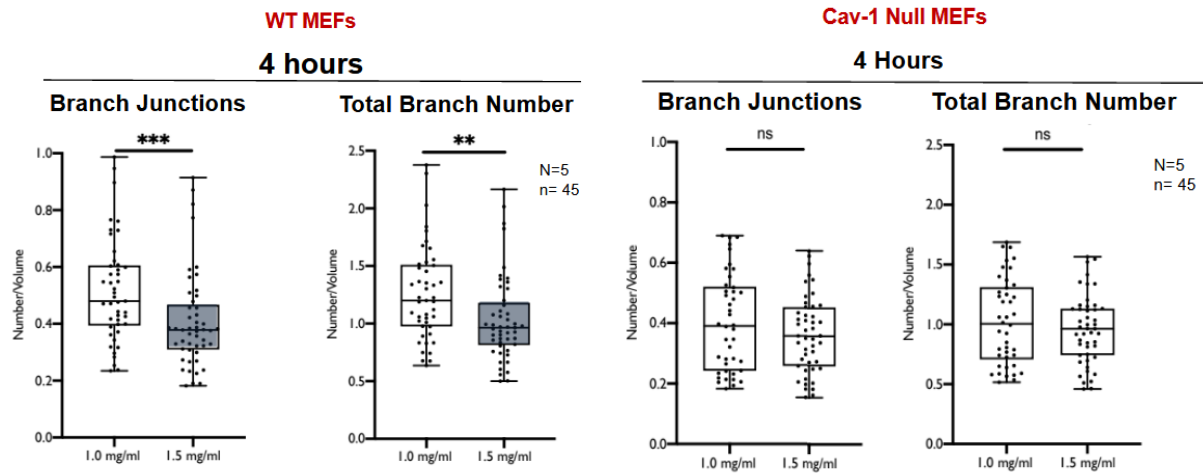
Figure 4.5: Figure shows two plots. The left plot shows the stiffness difference even when cells are round that is when the coverslip is coated with poly l lysine. The right plot shows plot that confirms at the 0.25uM Lat A the stiffness of both are same. This information will be used in further analysis.

Wild-type Mouse Embryonic Fibroblasts (WT MEFs) and Caveolin-1 null MEFs (Cav-1 Nulls) were embedded within 3D collagen matrices at two different concentrations. After 4 hours of incubation, the branching number and branch junctions of the collagen matrix near the embedded cells were analyzed. Debasmita Mazumdar calculated the branch number and branch junctions within the collagen matrix in the vicinity of the embedded cells. The results, presented in Figure 4.6, reveal distinct trends for WT MEFs and Cav-1 Nulls.

Embedding WT MEFs in the collagen matrix resulted in concentration-dependent changes in branch number and junctions. At the higher concentration, both the branch number and junctions were lower compared to the lower concentration.

In contrast to WT MEFs, embedding Cav-1 Nulls did not show any significant difference in branch number or junctions across the two collagen concentrations. The observed differences between WT MEFs and Cav-1 Nulls suggest that caveolin-1 might play a role in regulating cell-matrix interactions and their subsequent influence on collagen organization. From this observation we can comment that Cav 1 Nulls cannot sense the change in microenvironment and

hence on changing the concentration of collagen cell the branch number and branch junctions remained unchanged.

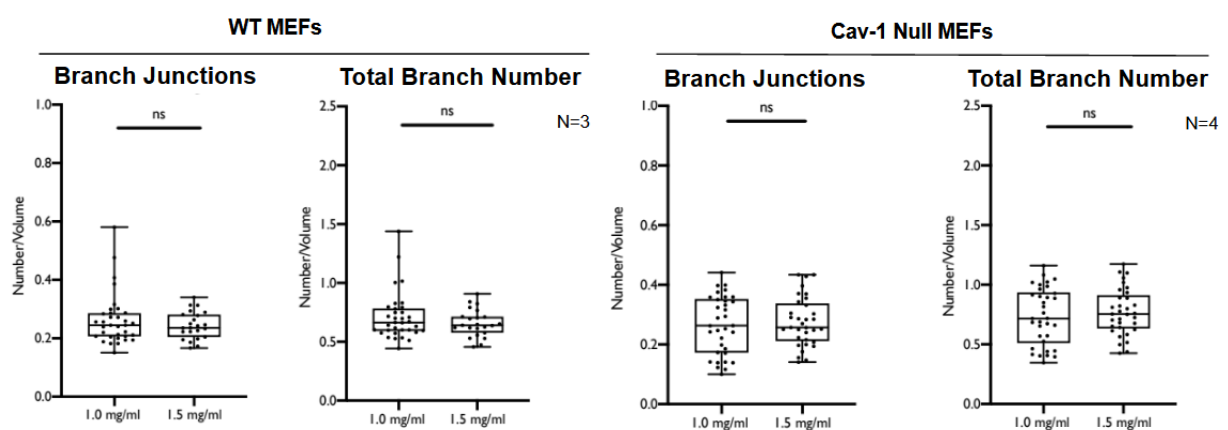


(a) Fig. shows comparison of Branch Numbers and (b) Fig. shows comparison of Branch Numbers and Junctions with WT MEFs on different concentration Junctions with Cav 1 Null MEFs on different concentration of collagen gel

Figure 4.6: Figure shows that for WT MEFs at the higher concentration, both the branch number and junctions were lower compared to the lower concentration on the other hand embedding Cav-1 Nulls did not show any significant difference in branch number or junctions across the two collagen concentrations. Figure Credits: Debasmita Mazumdar from Dr Nagraj Lab

Building upon the previous observations, we further investigated the influence of Latrunculin A treatment on the organization of collagen of different concentrations. WT MEFs and Cav-1 Nulls treated with Latrunculin A embedded within 3D collagen matrices at two different concentrations.

Similar to the previous experiment, branch number junctions within the collagen matrix near the embedded cells were analyzed after 4 hours of incubation. The results, presented in Figure 4.7, demonstrate that both WT MEFs and Cav-1 Nulls treated with Latrunculin A did not exhibit any significant difference in branch number or junctions across the two collagen concentrations. Note that the concentration of Lat A used was such that the stiffness of both WT and Cav 1 Nulls were same. Interestingly this pattern is comparable to the control scenario where no cells were embedded within the gel. We can comment that Latrunculin A treatment might disrupt the ability of both WT MEFs and Cav-1 Nulls to modulate collagen branching. Disruption of the actin cytoskeleton by Latrunculin A could potentially hinder the cellular processes involved in exerting mechanical forces or interacting with the surrounding matrix, leading to a lack of influence on branching patterns regardless of cell type or matrix density.



(a) Fig. shows comparison of Branch Numbers and (b) Fig. shows comparison of Branch Numbers and Junctions with embedded WT MEFs Lat A treated Junctions with embedded Cav 1 Null MEFs Lat A in two different concentration of collagen gel treated in two different concentration of collagen gel

Figure 4.7: Figure shows that for WT MEFs and Cav-1 Nulls both treated with Lat A did not show any significant difference in branch number or junctions across the two collagen concentrations and is comparable as there was no cell embedded inside the gel. Figure Credits: Debasmita Mazumdar from Dr Nagraj Lab



## Chapter 5

### CONCLUSION

This section contains conclusions of projects done for completion of my MS thesis. However, it is imperative to acknowledge that these conclusions represent but a fraction of the insights yet to be unearthed. As our journey progresses, propelled by ongoing advanced analyses, the vistas of comprehension promise to expand exponentially.

#### **Project 1: Molecular interaction of SARS-CoV-2 mutants binding to the human ACE2 receptor using AFM**

Through AFM experiments and analysis using Bell-Evans Model, we have successfully determined the dissociation constants (kinetic off rates) for mutants of the SARS-CoV-2 virus, specifically the Wuhan and Omicron variants, that yield  $K_{off}(\text{Wuhan}) = 1.961$  per sec and  $K_{off}(\text{Omicron}) = 0.389$  per sec. These findings highlight that the dissociation rate of the Omicron variant is significantly lower than that of the Wuhan variant, suggesting a more robust binding affinity between the Spike and ACE-2 receptor for Omicron. This insight underscores the importance of understanding variant-specific interactions in the development of effective vaccines. Looking ahead, the methodology employed in this study offers a valuable framework for comparative analysis of dissociation rates across a broader spectrum of variants just by changing the protein on the cantilever, and the rest protocol remains the same. Such investigations hold promise for informing the strategic development of vaccines tailored to evolving viral strains, thereby contributing to more intelligent and proactive public health measures.

#### **Project 2: Viscoelastic measurements of L Cells and their Clathrin Light Chain Knockout Variants using AFM Nanoindentation**

Till now, the investigation has yielded the basic knowledge of elastic and viscoelastic properties of L cells alongside their clathrin light chain knockout phenotypes. Our analysis with AFM and reflectance imaging data sheds light on the cellular dynamics following the disruption of clathrin light chains. Our findings indicate a notable shift in actin distribution within the cells subsequent to clathrin light chain knockout. Specifically, the displacement of actin from its

original position correlates with alterations in cellular elasticity. AFM data also supports this phenomenon, revealing a decrease in stiffness upon the knockout of individual light chains. However, the simultaneous knockout of both light chains reverses this trend, wherein actin repositions towards the cell centre increase cellular stiffness. These observations underscore the intricate interplay between clathrin-mediated processes and the cytoskeletal architecture, further illuminating the mechanistic underpinnings of cellular biomechanics.

### **Project 3: Quantitative evaluation of collagen organisation and its regulation by mouse fibroblasts in 3D hydrogels using AFM**

Wild-type Mouse Embryonic Fibroblasts (WT MEFs) and Caveolin-1 null MEFs (Cav-1 Nulls) were embedded within 3D collagen matrices at two different concentrations. After 4 hours of incubation, the collagen matrix's branching number and branch junctions near the embedded cells were analysed. Debasmita Mazumdar calculated the branch number and branch junctions within the collagen matrix in the vicinity of the embedded cells. The results reveal distinct trends for WT MEFs and Cav-1 Nulls. Embedding WT MEFs in the collagen matrix resulted in concentration-dependent changes in branch number and junctions. At the higher concentration, the branch number and junctions were lower than at the lower concentration. In contrast to WT MEFs, embedding Cav-1 Nulls did not show any significant difference in branch number or junctions across the two collagen concentrations. The observed differences between WT MEFs and Cav-1 Nulls suggest that caveolin-1 might regulate cell-matrix interactions and their subsequent influence on collagen organisation. From this observation, we can comment that Cav-1 Nulls cannot sense the change in the microenvironment and hence, on changing the concentration of collagen cells the branch number and branch junctions remained unchanged. Cav-1 Nulls did not show any significant difference in branch number or junctions across the two collagen concentrations. Building upon the previous observations, we further investigated the influence of Latrunculin A treatment on the organisation of collagen of different concentrations. WT MEFs and Cav-1 Nulls treated with Latrunculin A were embedded within 3D collagen matrices at two different concentrations. Similar to the previous experiment, branch number junctions within the collagen matrix near the embedded cells were analysed after 4 hours of incubation. The results demonstrate that WT MEFs and Cav-1 Nulls treated with Latrunculin A did not exhibit any significant difference in branch number or junctions across the two collagen concentrations. Note that the concentration of Lat A used was such that the stiffness of both WT and Cav-1 Nulls were the same. Interestingly, this pattern is comparable to the control scenario, where no cells were embedded within the gel. We can comment that Latrunculin A treatment might disrupt the ability of WT MEFs and Cav-1 Nulls to modulate collagen branching. Disruption of the actin cytoskeleton by Latrunculin A could potentially hinder the cellular

processes involved in exerting mechanical forces or interacting with the surrounding matrix, leading to a lack of influence on branching patterns regardless of cell type or matrix density.

## BIBLIOGRAPHY

- [1] Arthur Ashkin, James M Dziedzic, John E Bjorkholm, and Steven Chu. Observation of a single-beam gradient force optical trap for dielectric particles. *Optics letters*, 11(5):288–290, 1986.
- [2] George I Bell. Models for the specific adhesion of cells to cells: a theoretical framework for adhesion mediated by reversible bonds between cell surface molecules. *Science*, 200(4342):618–627, 1978.
- [3] Gerd Binnig, Calvin F Quate, and Ch Gerber. Atomic force microscope. *Physical review letters*, 56(9):930, 1986.
- [4] Gerd Binnig, Heinrich Rohrer, Ch Gerber, and Edmund Weibel. Surface studies by scanning tunneling microscopy. *Physical review letters*, 49(1):57, 1982.
- [5] Arno R Bourgonje, Amaal E Abdulle, Wim Timens, Jan-Luuk Hillebrands, Gerjan J Navis, Sanne J Gordijn, Marieke C Bolling, Gerard Dijkstra, Adriaan A Voors, Albert DME Osterhaus, et al. Angiotensin-converting enzyme 2 (ace2), sars-cov-2 and the pathophysiology of coronavirus disease 2019 (covid-19). *The Journal of pathology*, 251(3):228–248, 2020.
- [6] Carlos Bustamante, Lisa Alexander, Kevin Maciuba, and Christian M Kaiser. Single-molecule studies of protein folding with optical tweezers. *Annual review of biochemistry*, 89:443–470, 2020.
- [7] Natasha Buwa and Nagaraj Balasubramanian. Extracellular matrix–dependent mechanosensing and mechanotransduction: role in cell migration. In *Cell Movement in Health and Disease*, pages 101–127. Elsevier, 2022.
- [8] Natasha Buwa, Debasmita Mazumdar, and Nagaraj Balasubramanian. Caveolin1 tyrosine-14 phosphorylation: role in cellular responsiveness to mechanical cues. *The Journal of Membrane Biology*, 253:509–534, 2020.
- [9] Hu Chen, Hongxia Fu, Xiaoying Zhu, Peiwen Cong, Fumihiko Nakamura, and Jie Yan. Improved high-force magnetic tweezers for stretching and refolding of proteins and short dna. *Biophysical journal*, 100(2):517–523, 2011.

- [10] Jyoti Das, Mahak Tiwari, and Deepa Subramanyam. Clathrin light chains: Not to be taken so lightly. *Frontiers in Cell and Developmental Biology*, 9:774587, 2021.
- [11] Iwijn De Vlaminck and Cees Dekker. Recent advances in magnetic tweezers. *Annual review of biophysics*, 41:453–472, 2012.
- [12] Gary J Doherty and Harvey T McMahon. Mechanisms of endocytosis. *Annual review of biochemistry*, 78:857–902, 2009.
- [13] Yuri M Efremov, Takaharu Okajima, and Arvind Raman. Measuring viscoelasticity of soft biological samples using atomic force microscopy. *Soft matter*, 16(1):64–81, 2020.
- [14] Tony Fischer, Alexander Hayn, and Claudia Tanja Mierke. Effect of nuclear stiffness on cell mechanics and migration of human breast cancer cells. *Frontiers in cell and developmental biology*, 8:393, 2020.
- [15] Ikuko Fujiwara, Mark E Zweifel, Naomi Courtemanche, and Thomas D Pollard. Latrunculin a accelerates actin filament depolymerization in addition to sequestering actin monomers. *Current Biology*, 28(19):3183–3192, 2018.
- [16] Thomas M Gallagher and Michael J Buchmeier. Coronavirus spike proteins in viral entry and pathogenesis. *Virology*, 279(2):371, 2001.
- [17] Franz J Giessibl. A direct method to calculate tip–sample forces from frequency shifts in frequency-modulation atomic force microscopy. *Applied Physics Letters*, 78(1):123–125, 2001.
- [18] Jeffrey L Hutter and John Bechhoefer. Calibration of atomic-force microscope tips. *Review of scientific instruments*, 64(7):1868–1873, 1993.
- [19] Seonghan Kim, Yi Liu, Matthew Ziarnik, Sangjae Seo, Yiwei Cao, X Frank Zhang, and Wonpil Im. Binding of human ace2 and rbd of omicron enhanced by unique interaction patterns among sars-cov-2 variants of concern. *Journal of computational chemistry*, 44(4):594–601, 2023.
- [20] Michael M Lacy, Rui Ma, Neal G Ravindra, and Julien Berro. Molecular mechanisms of force production in clathrin-mediated endocytosis. *FEBS letters*, 592(21):3586–3605, 2018.
- [21] Jean-Léon Maître and Carl-Philipp Heisenberg. Three functions of cadherins in cell adhesion. *Current Biology*, 23(14):R626–R633, 2013.

- [22] Majid Moshirfar, Lawsen Parker, Orry C Birdsong, Yasmyne C Ronquillo, Daniel Hofstedt, Tirth J Shah, Aaron T Gomez, C Phillip Sr, et al. Use of rho kinase inhibitors in ophthalmology: a review of the literature. *Medical Hypothesis, Discovery and Innovation in Ophthalmology*, 7(3):101, 2018.
- [23] Ridim D Mote, Jyoti Yadav, Surya Bansi Singh, Mahak Tiwari, Shivprasad Patil, Deepa Subramanyam, et al. Pluripotency of embryonic stem cells lacking clathrin-mediated endocytosis cannot be rescued by restoring cellular stiffness. *Journal of Biological Chemistry*, 295(49):16888–16896, 2020.
- [24] Xiaocong Pang, Xu He, Zhiwei Qiu, Hanxu Zhang, Ran Xie, Zhiyan Liu, Yanlun Gu, Nan Zhao, Qian Xiang, and Yimin Cui. Targeting integrin pathways: mechanisms and advances in therapy. *Signal Transduction and Targeted Therapy*, 8(1):1, 2023.
- [25] Jessica Planade, Reda Belbahri, Micaela Boiero Sanders, Audrey Guillotin, Olivia Du Roure, Alphée Michelot, and Julien Heuvingh. Mechanical stiffness of reconstituted actin patches correlates tightly with endocytosis efficiency. *PLoS biology*, 17(10):e3000500, 2019.
- [26] Christian Rankl, Linda Wildling, Isabel Neundlinger, Ferry Kienberger, Hermann Gruber, Dieter Blaas, and Peter Hinterdorfer. Determination of the kinetic on-and off-rate of single virus–cell interactions. *Atomic Force Microscopy in Biomedical Research: Methods and Protocols*, pages 197–210, 2011.
- [27] Aashrith Saraswathibhatla, Dhiraj Indana, and Ovijit Chaudhuri. Cell–extracellular matrix mechanotransduction in 3d. *Nature Reviews Molecular Cell Biology*, 24(7):495–516, 2023.
- [28] Surya Bansi Singh, Shatruhan Singh Rajput, Shivprasad Patil, and Deepa Subramanyam. Protocol for measuring mechanical properties of live cells using atomic force microscopy. *STAR protocols*, 5(1):102870, 2024.
- [29] Maria Cristina Tanzi and Silvia Farè. Adipose tissue engineering: state of the art, recent advances and innovative approaches. *Expert review of medical devices*, 6(5):533–551, 2009.
- [30] M Alejandra Tortorici and David Veesler. Structural insights into coronavirus entry. In *Advances in virus research*, volume 105, pages 93–116. Elsevier, 2019.
- [31] Mei-Yue Wang, Rong Zhao, Li-Juan Gao, Xue-Fei Gao, De-Ping Wang, and Ji-Min Cao. Sars-cov-2: structure, biology, and structure-based therapeutics development. *Frontiers in cellular and infection microbiology*, 10:587269, 2020.

- [32] Kenneth M Yamada, Andrew D Doyle, and Jiaoyang Lu. Cell–3d matrix interactions: recent advances and opportunities. *Trends in cell biology*, 32(10):883–895, 2022.
- [33] Renhong Yan, Yuanyuan Zhang, Yaning Li, Lu Xia, Yingying Guo, and Qiang Zhou. Structural basis for the recognition of sars-cov-2 by full-length human ace2. *Science*, 367(6485):1444–1448, 2020.
- [34] Jinsung Yang, Simon JL Petitjean, Melanie Koehler, Qingrong Zhang, Andra C Dumitru, Wenzhang Chen, Sylvie Derclaye, Stéphane P Vincent, Patrice Soumillion, and David Alsteens. Molecular interaction and inhibition of sars-cov-2 binding to the ace2 receptor. *Nature communications*, 11(1):4541, 2020.
- [35] Peng Zhou, Xing-Lou Yang, Xian-Guang Wang, Ben Hu, Lei Zhang, Wei Zhang, Hao-Rui Si, Yan Zhu, Bei Li, Chao-Lin Huang, et al. A pneumonia outbreak associated with a new coronavirus of probable bat origin. *nature*, 579(7798):270–273, 2020.